A stress-dependent TRIM28–ALKBH2 feedback loop modulates chemoresistance in NSCLC

Zhiming Sun,[1] Yunfang Deng,[1] Yue Liu,[1] Zhaohui Liu,[1] Jiabing Li,[1] Lihui Wu,[1] Liyuan Zeng,[1] Xiaorong Feng,[1] Lin Miao,[1] Ying Sheng,[1] Bei Chen,[1] Yuming He,[1] Ye Liu[1] & Yu Zhao[1,2*]

[1]The National & Local Joint Engineering Laboratory of Animal Peptide Drug Development, College of Life Sciences, Hunan Normal University, Changsha, Hunan, 410081, China

[2]Peptide and Small Molecule Drug R&D Platform, Furong Laboratory, Hunan Normal University, Changsha, Hunan, 410081, China

* Corresponding author: Yu Zhao (smile_zhao@hotmail.com)

Running title: TRIM28–ALKBH2 feedback loop modulates chemoresistance

Keywords: TRIM28, ALKBH2, MAGEA6, Ubiquitination, Chemoresistance

ABSTRACT

Chemoresistance to DNA-damaging agents, including platinum and alkylating compounds, limits treatment efficacy in non-small cell lung cancer (NSCLC) and is frequently associated with elevated DNA repair activity. Here, we identify a stress-responsive feedback loop between the E3 ligase TRIM28 and the demethylase ALKBH2. TRIM28 binds ALKBH2 and promotes its K48-linked polyubiquitination and proteasomal degradation, whereas ALKBH2 enhances TRIM28 transcription and protein levels, forming a feedback loop. Notably, alkylation stress induces a biphasic response: acute MMS exposure enhances TRIM28–ALKBH2 association and accelerates ALKBH2 degradation, whereas prolonged exposure promotes TRIM28 degradation, leading to ALKBH2 stabilization and transcriptional upregulation. Clinically, ALKBH2 is frequently elevated in lung adenocarcinoma and is associated with worse survival, whereas TRIM28 exhibits prognostic value specifically in chemotherapy-treated patients. Functionally, MMS–cisplatin co-treatment increased DNA damage and reduced clonogenic survival by counteracting ALKBH2-dependent alkylation tolerance, linking the TRIM28–ALKBH2 loop to chemoresistance in NSCLC.

Introduction

Cells are continuously exposed to endogenous metabolites and exogenous alkylating agents that induce cytotoxic and mutagenic DNA adducts, posing a persistent threat to genome integrity (*1, 2*). These lesions are repaired through three principal mechanisms: base excision repair (BER), direct reversal by O^6-methylguanine-DNA methyltransferase (MGMT), and oxidative demethylation catalyzed by AlkB family of Fe(II)/α-ketoglutarate–dependent dioxygenases (*3-5*). AlkB enzymes remove N-linked methyl lesions such as 1-meA and 3-meC via a coupled oxidative reaction that restores the native base (*6-8*). In mammalian cells, these dioxygenases function alongside BER and MGMT to resolve lesions that escape other repair pathways, thereby contributing to genome maintenance across diverse cellular contexts. Changes in AlkB expression or stability are associated with distinct cellular responses to alkylation damage, emphasizing the need for proper regulation of this repair axis.

Although AlkB family enzymes are subject to transcriptional and epigenetic regulation (*9-12*), accumulating evidence indicates that AlkB family dioxygenase protein levels are controlled by ubiquitin-dependent proteostasis. Ubiquitin-regulatory networks have been well characterized for several AlkB family homologues, most notably FTO and ALKBH5. FTO turnover is regulated by multiple context-dependent E3 ligases, including TRIM17, DTX2, MIB1, and RNF144A, and is further modulated by TRIM21 following O-GlcNAc–primed modification (*13-17*). ALKBH5 stability is similarly regulated by the E3 ligase RNF180 and by PRMT5-dependent methylation, the latter promoting its recognition by TRIM28 (*18, 19*). These degradative pathways are counterbalanced by substrate-specific deubiquitinases (DUBs), including USP7 and USP18 for FTO (*20, 21*), and USP14 and USP36 for ALKBH5 (*22, 23*). OTUD4 has also been reported to stabilize the related demethylase ALKBH3 through a noncanonical scaffolding DUB mechanism (*2*), consistent with ubiquitin-dependent regulation observed across multiple AlkB-family enzymes. However, whether this ubiquitin-dependent regulatory paradigm extends to all AlkB family members remains incompletely understood.

Among the nine mammalian AlkB homologues, ALKBH2 functions as a major demethylase involved in the repair of methylated bases in duplex DNA and in limiting alkylation-induced mutagenesis (*24-27*). ALKBH2 is frequently upregulated in cancer, particularly in non–small cell lung cancer (NSCLC), where its elevated expression is associated with increased tolerance to DNA damage and reduced sensitivity to DNA-damaging chemotherapeutic agents, including alkylating and platinum-based drugs (*26, 28-30*). Given that alkylating chemotherapeutics, such as temozolomide, and environmental exposures, including cigarette smoke, generate overlapping classes of methylated DNA lesions (*1, 31, 32*), sustained alkylation stress imposes selective pressure on pathways regulating ALKBH2 protein levels (*10, 33*). However, the ubiquitin-dependent mechanisms regulating ALKBH2 stability—including whether ALKBH2 undergoes ubiquitination and the identity of the E3 ligases or DUBs involved—remain incompletely defined. The ALKBH2-associated ASCC complex recruits TRIM28 upon MMS-induced alkylation stress (*34*), positioning TRIM28 within the alkylation repair context and suggesting a potential regulatory link between TRIM28 and ALKBH2.

The tripartite motif (TRIM) family of RING-type E3 ligases, including TRIM28 and TRIM24, plays a central role in ubiquitin signaling, integrating chromatin regulation with cellular stress responses (*35, 36*). TRIM28 utilizes its N-terminal RING domain and C-terminal PHD–BRD module to mediate KRAB-ZNF–dependent transcriptional silencing, contributing to the maintenance of genomic stability (*37, 38*). This modular architecture enables TRIM28 to function both as a transcriptional corepressor and an E3 ligase, with its activity and chromatin engagement dynamically regulated. In response to DNA double-strand breaks, TRIM28 undergoes ATM/ATR-dependent phosphorylation at Ser824, which relaxes heterochromatin and facilitates the recruitment of repair factors (*39, 40*). TRIM28 expression is further regulated by transcriptional and post-transcriptional programs, as well as by ubiquitin-dependent turnover under genotoxic or metabolic stress (*41-43*). Following DNA double-strand breaks, RNF4 targets TRIM28 for SUMOylation-dependent degradation (*44*). In parallel, under metabolic stress, March5 promotes TRIM28 ubiquitination and reduces its protein stability (*45*). Moreover, MAGE family proteins,

85 including MAGEA6, serve as cofactors that promote TRIM28 recruitment to its substrates by
86 facilitating the assembly of TRIM28–substrate E3 complexes (*46, 47*). Although multiple
87 regulatory layers of TRIM28 have been described, whether and how TRIM28 participates in
88 alkylation damage repair, and how its regulation is modulated under alkylating stress, remain
89 poorly understood.

90 In this study, we identify a stress-responsive feedback loop involving TRIM28, its cofactor
91 MAGEA6, and the DNA demethylase ALKBH2. TRIM28 binds ALKBH2 and promotes its K48-
92 linked polyubiquitination and proteasomal degradation, whereas ALKBH2 reciprocally enhances
93 TRIM28 transcription and protein levels. This loop is modulated by alkylation damage in a time-
94 dependent manner: short-term alkylation exposure enhances TRIM28–ALKBH2 association and
95 accelerates ALKBH2 degradation, whereas prolonged MMS exposure promotes TRIM28
96 ubiquitination and degradation, leading to ALKBH2 stabilization and enhanced transcription.
97 These data offer insights into how alkylation stress duration and context regulate ALKBH2
98 availability and modulate DNA repair capacity and chemoresistance in NSCLC.

Results

TRIM28 directly binds ALKBH2

To explore proteins associated with TRIM28, we performed tandem affinity purification in H1299 non–small cell lung cancer (NSCLC) cells, followed by silver staining and LC–MS/MS analysis. ALKBH2 was identified as a candidate TRIM28-associated protein (Fig. 1A, fig. S1A, and table S1). Co-immunoprecipitation (co-IP) assays in HEK293T cells coexpressing HA-tagged ALKBH2 and Flag-tagged TRIM28 confirmed this interaction, whereas no detectable association was observed with the related paralog TRIM24 (Fig. 1B). Reciprocal co-IP using HA-ALKBH2 further validated the specificity of the interaction (Fig. 1C).

To determine the TRIM28 region required for ALKBH2 binding, we performed domain-mapping analyses using a series of TRIM28 truncation mutants. These experiments indicated that the BCC region (B-box plus coiled-coil; residues 141–400) is required for ALKBH2 association (Fig. 1, D and E). ALKBH2 co-precipitated with TRIM28 in endogenous co-IP experiments, indicating that the interaction occurs under physiological conditions (Fig. 1F). Moreover, immunofluorescence analysis revealed prominent nuclear colocalization of TRIM28 and ALKBH2 (Fig. 1G).

In vitro MBP pull-down assays using purified recombinant proteins showed that TRIM28 directly binds ALKBH2 (Fig. 1H). Specificity assays revealed stronger binding to ALKBH2 than to ALKBH3 (Fig. 1I) or the direct-reversal repair enzyme MGMT (fig. S1B). Protein–protein docking predicted a TRIM28–ALKBH2 interface that overlaps the nucleic-acid-binding region of ALKBH2, centered on the Finger (hairpin) motif and the flexible Long-loop (*48*), which are present in ALKBH2 but absent in ALKBH3 (Fig. 1J). Consistent with this model, single-stranded DNA (ssDNA) competitively reduced TRIM28–ALKBH2 binding in a dose-dependent manner (Fig. 1K), a commonly used approach to assess the DNA-occupied states of repair enzymes (*49-51*). Collectively, these data indicate that TRIM28 directly binds ALKBH2 through its BCC domain and propose a mechanism in which DNA binding limits TRIM28 access to the ALKBH2 interaction interface.

126 **A reciprocal TRIM28–ALKBH2 regulatory loop coordinates ALKBH2 ubiquitination and**
127 **stability, with ALKBH2 enhancing TRIM28 transcription**

128 To determine whether ALKBH2 undergoes ubiquitin-dependent modification, we performed
129 denaturing immunoprecipitation (IP) of Flag-ALKBH2 from HEK293T cells co-transfected with
130 HA-ubiquitin (Ub). A high-molecular-weight smear corresponding to polyubiquitinated ALKBH2
131 was detected and was markedly increased upon proteasome inhibition with MG132 (Fig. 2A).
132 Expression of a K48-only ubiquitin mutant further enhanced ALKBH2 ubiquitination, whereas the
133 K48R ubiquitin mutant almost completely abolished it (Fig. 2B), suggesting that ALKBH2 is
134 primarily modified by K48-linked polyubiquitin chains. Halo-TUBE pull-down assays confirmed
135 that endogenous ALKBH2 undergoes K48-linked polyubiquitination (Fig. 2C).

136 We next examined whether TRIM28 mediates ALKBH2 ubiquitination. Overexpression of
137 wild-type (WT) TRIM28 increased K48-linked ubiquitination of ALKBH2 (Fig. 2D), whereas the
138 RING-inactive C65/68A mutant, which abolishes TRIM28 E3 ligase activity (*46*), did not enhance
139 ALKBH2 ubiquitination (Fig. 2E). TRIM28 depletion using two independent shRNAs markedly
140 reduced ALKBH2 ubiquitination (fig. S2A), and re-expression of shRNA-resistant TRIM28
141 restored this activity (Fig. 2F). These data indicate that TRIM28 E3 ligase activity is required to
142 promote efficient K48-linked ubiquitination of ALKBH2.

143 We then examined whether TRIM28 regulates ALKBH2 protein stability. TRIM28
144 knockdown in H1299 and A549 cells increased ALKBH2 protein levels without altering its mRNA
145 expression (Fig. 2, G and H). This effect was reproduced by CRISPR/Cas9-mediated TRIM28
146 depletion (fig. S2B). Conversely, increasing TRIM28 expression led to a dose-dependent decrease
147 in ALKBH2 protein levels in both H1299 and HEK293T cells (Fig. 2I). Cycloheximide (CHX)
148 chase assays showed that TRIM28 knockout extended the half-life of ALKBH2, whereas TRIM28
149 overexpression shortened it in a RING-dependent manner (fig. S2, C to F). Notably, these changes
150 occurred without altering ALKBH2 subcellular localization (fig. S2G). These data indicate that
151 TRIM28 regulates ALKBH2 protein stability by promoting its degradation.

152 To determine whether ALKBH2 in turn regulates its E3 ligase, we depleted ALKBH2 in
153 H1299 cells using two independent shRNAs. TRIM28 protein levels were reduced following
154 ALKBH2 knockdown (Fig. 2J), and re-expression of Flag-ALKBH2 restored TRIM28 protein
155 levels (Fig. 2K). In parallel, ALKBH2 overexpression increased TRIM28 mRNA levels as
156 measured by qRT-PCR (Fig. 2L). Consistent with this regulatory relationship, analysis of TCGA
157 lung adenocarcinoma datasets revealed a positive correlation between ALKBH2 and TRIM28
158 transcript levels (fig. S2H). Collectively, these data identify a feedback loop in which TRIM28
159 promotes K48-linked ubiquitination and proteasome-dependent degradation of ALKBH2, whereas
160 ALKBH2 enhances TRIM28 transcription and protein levels.
161

162 **MAGEA6 enhances TRIM28 E3 ligase assembly and activity toward ALKBH2, a function**
163 **impaired by cancer-associated variants**

164 MAGE family proteins interact with TRIM-type E3 ligases to modulate their activity (*46, 52*). To
165 assess how MAGEA6 contributes to the organization of the TRIM28–ALKBH2 complex, we
166 examined whether MAGEA6 associates with ALKBH2. Co-IP in HEK293T cells revealed an
167 association between MAGEA6 and ALKBH2 (Fig. 3A), and pull-down assays using purified
168 proteins confirmed a direct interaction (Fig. 3B). TRIM28 depletion did not affect MAGEA6–
169 ALKBH2 binding (Fig. 3C), suggesting that this interaction occurs independently of TRIM28.
170 MAGEA6 overexpression enhanced TRIM28–ALKBH2 association in a dose-dependent manner
171 (Fig. 3D and fig. S3A), whereas knockdown of endogenous MAGEA3/6 attenuated this interaction
172 (Fig. 3E); MAGEA3 and MAGEA6 were analyzed collectively due to their 96% sequence
173 homology (*53*). Furthermore, the related protein MAGEC2 also enhanced TRIM28–ALKBH2
174 assembly (fig. S3B), consistent with a conserved role of MAGEA/C family members in
175 orchestrating this complex.

176 We next examined whether MAGEA6 regulates TRIM28-dependent ubiquitination and
177 turnover of ALKBH2. MAGEA6 knockdown reduced endogenous ALKBH2 ubiquitination,
178 whereas re-expression of MAGEA6 reversed this modification (fig. S3C). Conversely, MAGEA6

179 overexpression promoted K48-linked ubiquitination of ALKBH2, an effect that was abolished
180 upon TRIM28 depletion (Fig. 3F), indicating a TRIM28-dependent requirement for MAGEA6 in
181 ALKBH2 ubiquitination. Notably, MAGEA6 promoted ALKBH2 degradation in control cells,
182 whereas this effect was not observed in TRIM28-knockout H1299 cells (Fig. 3, G and H).

183 Cancer-associated variants in MAGEA6 have been reported across multiple tumor types,
184 including lung cancer (*54*). We therefore analyzed endogenous MAGEA6 transcripts in H1299
185 cells and identified two variants, MutA and MutB, harboring 12 and 20 amino acid substitutions,
186 respectively (Fig. S3D). Both variants were cloned and sequence-verified. Co-IP assays revealed
187 that both MutA and MutB showed reduced interaction with ALKBH2, whereas MutB additionally
188 reduced interaction with TRIM28 (Fig. 3I). Consistent with these binding defects, both variants
189 were less effective than wild-type MAGEA6 at enhancing ALKBH2 ubiquitination and
190 degradation (Fig. 3J and fig. S3E).

191 To explore the structural basis of this interaction, AlphaFold3 modeling identified a putative
192 TRIM28-binding interface within the MAGE homology domain involving residues D156 and
193 S157 (fig. S3F). Within this interface, S157 is substituted in the MutB variant and overlaps with
194 tumor-associated substitutions reported in COSMIC for MAGEA6 and the homologous MAGEA3.
195 Structure-guided mutagenesis further showed that an interface-disrupting D156E/S157Y double
196 substitution reduced association with TRIM28 and decreased MAGEA6-dependent ALKBH2
197 stability (Fig. 3K and fig. S3G). In contrast, the K211R substitution—located within the predicted
198 ALKBH2-binding surface—had minimal effect on MAGEA6–ALKBH2 interaction (Fig. 3K).
199 Collectively, these data indicate that residues D156 and S157 contribute to the MAGEA6–
200 TRIM28 interface and that disruption of this interface impairs MAGEA6-dependent ALKBH2
201 ubiquitination and degradation. This conclusion is consistent with the enrichment of tumor-
202 associated variants at this site.

203

204 **MMS drives a biphasic ALKBH2 response, from acute degradation to prolonged**
205 **accumulation**

206 **MMS acutely promotes ALKBH2 degradation**

207 To investigate how MMS regulates the TRIM28–ALKBH2 axis, we examined their association
208 dynamics in H1299 cells. Short-term MMS exposure (3–6 h) increased the TRIM28–ALKBH2
209 association in a time- and dose-dependent manner (Fig. 4, A and B). Both TRIM28 and ALKBH2
210 were predominantly nuclear regardless of MMS treatment (fig. S4A). In contrast, MAGEA3/6
211 showed increased nuclear localization upon MMS exposure (Fig. 4C), consistent with the
212 involvement of MAGEA3/6 in enhanced TRIM28–ALKBH2 assembly during genotoxic stress.
213 Accordingly, MMS increased ALKBH2 K48-linked ubiquitination in a concentration-dependent
214 manner (Fig. 4D).

215 To exclude transcriptional effects, we used H1299 cells stably expressing TAP-tagged
216 ALKBH2 (Flag–HA tandem affinity tag). MMS accelerated ALKBH2 degradation, and this effect
217 was further potentiated by TRIM28 overexpression (Fig. 4E). Endogenous ALKBH2 similarly
218 showed reduced stability when cells were co-treated with MMS and cycloheximide (CHX),
219 compared with CHX alone (fig. S4, B and C). These data indicate an early response phase in which
220 MMS triggers TRIM28-dependent ubiquitination and degradation of ALKBH2.

221 Because alkylating agents such as MMS and temozolomide (TMZ) elevate intracellular ROS
222 (*55, 56*), we next examined whether redox conditions influence TRIM28–ALKBH2 association.
223 Co-IP analysis revealed that H_2O_2 enhanced this association, whereas ssDNA, ascorbate (Vc), or
224 EDTA reduced it (Fig. 4F). Reduced glutathione (GSH) diminished TRIM28–ALKBH2
225 association, whereas oxidized glutathione (GSSG) had minimal effect; GSH also attenuated the
226 H_2O_2-induced increase (fig. S4D). EDTA similarly lowered basal association and blocked H_2O_2-
227 driven enhancement (Fig. 4G). Notably, oxidative stress alone was sufficient to induce K48-linked
228 polyubiquitination of ALKBH2 (fig. S4E).

229 The catalytically inactive ALKBH2(H171A/D173A) mutant (*48, 57*), within the Fe(II)-
230 binding active site, was refractory to both the ssDNA-dependent reduction and the H_2O_2-induced
231 enhancement of TRIM28 binding, indicating that these redox-associated effects depend on
232 ALKBH2 catalytic activity (fig. S4F). The reducing agent Vc further suppressed MMS-induced

233 K48-linked ubiquitination of ALKBH2 (Fig. 4H). Together, these data indicate an acute, redox-
234 responsive phase in which TRIM28-mediated ubiquitination drives ALKBH2 degradation.

235 **Prolonged MMS exposure stabilizes ALKBH2**

236 In contrast to the early degradative phase, prolonged MMS exposure (≥8 h) progressively
237 increased ALKBH2 protein levels in H1299 and H460 cells (Fig. 4, I and J). In comparison, the
238 related demethylase ALKBH3 and MGMT showed no detectable change in protein levels under
239 the same conditions. TRIM28 overexpression attenuated the MMS-induced increase in ALKBH2
240 (Fig. 4K). Together, these results indicate that prolonged MMS exposure stabilizes ALKBH2.

241 **Prolonged MMS exposure induces transcriptional upregulation of ALKBH2**

242 To determine whether ALKBH2 accumulation involves transcriptional activation, we measured
243 ALKBH2 transcript levels in H1299 cells after MMS exposure for the indicated durations.
244 ALKBH2 mRNA increased at 12 h and remained elevated at 24 h (Fig. 4L), paralleling the delayed
245 increase in ALKBH2 protein levels.

246 Collectively, these data reveal a stress-dependent feedback loop, with an early TRIM28-
247 dependent ubiquitination and degradation phase, followed by a later phase characterized by
248 ALKBH2 stabilization accompanied by transcriptional induction.

249

250 **MMS induces K48-linked ubiquitination and proteasomal degradation of TRIM28,**
251 **coordinated by TRIM24 and MAGEA6**

252 To investigate how TRIM28 is regulated during alkylation stress, we examined its stability and
253 post-translational modification. MMS treatment caused a time- and dose-dependent decrease in
254 TRIM28 protein without altering its mRNA (Fig. 5, A to C), and this reduction was blocked by
255 MG132, consistent with proteasome-mediated degradation. Prolonged low-dose MMS exposure
256 (100 μM, 24–72 h) led to a progressive increase in ALKBH2 protein levels, whereas ALKBH3,
257 MGMT, and MAGEA3/6 remained stable (fig. S5A). A 12-h MMS pre-exposure caused TRIM28
258 depletion, increased basal ALKBH2 levels, and slower degradation of ALKBH2 (fig. S5, B and

259 C), indicating that reduced TRIM28 availability contributes to ALKBH2 accumulation during
260 sustained alkylation stress.

261 To examine the mechanism underlying this regulation, we analyzed TRIM28 ubiquitination.
262 Denaturing IP of Flag-TRIM28 revealed that MMS markedly induced TRIM28 polyubiquitination,
263 which increased over time in H1299 cells (Fig. 5, D and E). Use of a K48-only ubiquitin mutant
264 indicated that these conjugates are predominantly K48-linked (Fig. 5F). K48-specific Halo-TUBE
265 pulldown detected MMS-induced ubiquitination of endogenous TRIM28 (Fig. 5G). In contrast,
266 other genotoxic agents—including TMZ, CDDP, and H_2O_2—did not induce detectable K48-linked
267 ubiquitination or TRIM28 degradation (Fig. 5H and fig. S5, D to F), indicating that TRIM28
268 degradation is selective for MMS-induced alkylation stress. The SUMO-acceptor-site TRIM28
269 mutant (K554/779/804R) (*58*) exhibited impaired K48-linked ubiquitination (Fig. 5I), indicating
270 that this lysine cluster is required for efficient MMS-induced modification.

271 To identify upstream factors regulating TRIM28 turnover, we analyzed the TRIM28
272 interactome (table S2) and validated selected interacting proteins. MMS increased TRIM28
273 association with the E3 ligase TRIM24 and the proteasome subunits PSMD4 and PSMB5 in a
274 time-dependent manner (Fig. 5J), whereas these interactions were weakened in the SUMO-
275 acceptor mutant (fig. S5G). MAGEA6 further enhanced the assembly of the TRIM28–TRIM24
276 complex. Upon MMS exposure, MAGEA6 co-expression increased TRIM28 binding to TRIM24
277 and PSMD4/PSMB5, accompanied by enhanced K48-linked TRIM28 ubiquitination (Fig. 5K).
278 Reciprocal co-IP using Flag-TRIM24 confirmed the MMS-inducible TRIM28–TRIM24
279 interaction and revealed that TRIM24 itself undergoes K48-linked ubiquitination (Fig. 5L).
280 Overexpression of TRIM24 enhanced MMS-induced ubiquitination and accelerated the reduction
281 of endogenous TRIM28 (Fig. 5M and fig. S5, H and I). Collectively, these data indicate that MMS
282 induces K48-linked ubiquitination and proteasomal degradation of TRIM28 via a pathway
283 involving MAGEA6, TRIM24, and SUMO-dependent regulation.

284

285 **TRIM28–ALKBH2 axis links patient outcome to alkylation-stress responses**

286 To assess the clinical relevance of this pathway in lung adenocarcinoma (LUAD), we examined
287 expression patterns of key alkylation repair enzymes. Analysis of TCGA transcriptomic and
288 CPTAC proteomic datasets indicated increased ALKBH2 and decreased ALKBH3 in tumors
289 relative to normal lung tissue, whereas MGMT showed no significant change (Fig. 6A and fig.
290 S6A). Immunohistochemistry further confirmed stronger ALKBH2 staining in LUAD than in
291 matched normal samples (Fig. 6B). A similar expression pattern was observed in NSCLC cell lines,
292 with higher ALKBH2 and lower ALKBH3 levels compared with BEAS-2B bronchial epithelial
293 cells (Fig. 6C). In survival analyses, elevated ALKBH2 was associated with worse overall survival,
294 whereas higher ALKBH3 correlated with improved prognosis (Fig. 6, D and E).

295 Because cigarette smoking generates alkylating and methylating DNA lesions (*59*), we next
296 analyzed ALKBH2 expression according to smoking status. ALKBH2 transcript levels were
297 higher in LUAD patients with a smoking history than in non-smokers (fig. S6B). Somatic
298 mutations in MAGEA6, a component of the TRIM28–ALKBH2 pathway, were also more frequent
299 in smokers, whereas MAGEA3 mutations showed no enrichment (fig. S6C). These observations
300 suggest an association between ALKBH2 expression and smoking-linked alkylation stress.

301 To examine the functional relevance of these clinical associations under alkylation stress, we
302 used an acute MMS exposure model. Because prolonged MMS treatment reduces TRIM28 and
303 induces delayed ALKBH2 accumulation, we used a brief high-dose MMS pulse (500 μM, 1 h) that
304 induced γ-H2AX with minimal effects on TRIM28 and ALKBH2 protein levels (fig. S6D). Under
305 these conditions, ALKBH2 knockdown reduced cell viability and enhanced MMS sensitivity (Fig.
306 6, F and G). TRIM28 overexpression did not alter basal proliferation (Fig. S6E) but enhanced
307 MMS sensitivity in a RING-dependent manner, and co-expression of ALKBH2 reversed this
308 sensitization (Fig. 6, H-J), indicating that ALKBH2 acts downstream of TRIM28 during acute
309 alkylation stress.

310 We next examined whether MAGEA6 modulates cellular sensitivity to alkylation stress.
311 MAGEA6 overexpression increased MMS sensitivity, whereas its knockdown reduced MMS
312 sensitivity. Re-expression of MAGEA6 restored MMS sensitivity (fig. S6F). MAGEA6 failed to

313 enhance MMS cytotoxicity when TRIM28 was depleted, and a TRIM28-binding–deficient mutant
314 (D156E/S157Y) exhibited a reduced sensitizing effect (Fig. 6, K and L). In contrast, MAGEA6
315 did not affect responses to cisplatin (CDDP) or the proteasome inhibitor bortezomib (fig. S6, G
316 and H), indicating that its regulatory effect is preferentially associated with alkylation stress rather
317 than broad cytotoxic stress. Collectively, these data indicate that MAGEA6 functions within the
318 TRIM28–ALKBH2 axis to regulate ALKBH2 during alkylation stress.
319

320 **TRIM28–ALKBH2 axis regulates MMS–CDDP combinatorial sensitivity**

321 To evaluate the clinical relevance of TRIM28, we analyzed 771 NSCLC cases. Among patients
322 who received systemic therapy, platinum-based regimens, predominantly cisplatin-containing
323 combinations, represented the major treatment modality (fig. S7A). High TRIM28 expression was
324 associated with worse overall survival in chemotherapy-treated patients, whereas no prognostic
325 association was observed in patients who did not receive chemotherapy (fig. S7, B and C). These
326 data indicate that TRIM28 expression associates with adverse prognosis, specifically in
327 chemotherapy-treated NSCLC patients.

328 To test whether TRIM28 influences cellular responses to sustained alkylation stress, we
329 established a chronic MMS exposure model. MMS IC_{50} values were approximately 141.5 μM in
330 H1299 cells and 236.8 μM in H460 cells (fig. S7D). In dose–response assays, H1299 cells were
331 exposed to MMS concentrations spanning the IC_{50} range (40–120 μM) for 48 h, and TRIM28
332 depletion increased MMS resistance (Fig. 7A). In long-term clonogenic assays, H460 cells were
333 treated with 100 μM MMS for 48 h and allowed to recover for 7 days in drug-free medium, and
334 TRIM28 overexpression increased MMS sensitivity and reduced colony formation (Fig. 7, B and
335 C). These results indicate that TRIM28 promotes cellular sensitivity to sustained MMS-induced
336 alkylation stress.

337 We next examined whether the TRIM28–ALKBH2 axis modulates cellular responses to
338 combined alkylating and platinum stress. For MMS–CDDP co-treatment, 2 μM CDDP was used
339 as a low-background dose because it was minimally cytotoxic as a single agent. TRIM28

340 overexpression reduced cell viability under MMS treatment, and MMS–CDDP co-treatment
341 further decreased viability (Fig. 7D). To assess the contribution of ALKBH2, we examined MMS
342 and CDDP sensitivity in cells with stable ALKBH2 knockdown to avoid confounding effects of
343 MMS-induced ALKBH2 upregulation. Re-expression of ALKBH2 restored MMS tolerance,
344 consistent with its role in alkylation repair. However, under MMS–CDDP co-treatment, low-dose
345 CDDP attenuated ALKBH2-mediated protection and increased MMS-induced cell death (Fig. 7E).
346 These results indicate that combined alkylating and platinum stress weakens ALKBH2-dependent
347 MMS tolerance in a TRIM28-dependent manner.

348 To explore mechanisms underlying reduced ALKBH2-mediated protection during MMS–
349 CDDP co-treatment, we assessed oxidative stress and DNA damage readouts. Because cisplatin
350 can induce reactive oxygen species, including H_2O_2 (*60*), we tested whether H_2O_2-mediated
351 oxidative stress enhances MMS cytotoxicity. Co-treatment of MMS with increasing
352 concentrations of H_2O_2 reduced cell viability in a dose-dependent manner (fig. S7E), consistent
353 with the enhanced cytotoxicity observed under MMS–CDDP co-treatment. Alkaline comet assays
354 indicated that low-dose CDDP (2 μM) or MMS (50 μM) alone induced limited DNA strand breaks,
355 whereas combined MMS–CDDP treatment increased tail moments (Fig. 7F) and γ-H2AX
356 accumulation (fig. S7F). These observations indicate that oxidative and alkylating stresses are
357 associated with increased DNA damage during MMS–CDDP co-treatment, which may contribute
358 to reduced ALKBH2-mediated protection.

359 Finally, we tested whether low-level alkylation stress alters cellular sensitivity to cisplatin.
360 Sub-IC_{50} MMS reduced the IC_{50} of CDDP in both H1299 and H460 cells (Fig. 7, G and H). In
361 colony formation assays, MMS–CDDP co-treatment further reduced clonogenic survival (Fig. 7,
362 I and J). In three-dimensional tumor spheroids, MMS–CDDP co-treatment similarly reduced
363 spheroid size and viability (Fig. 7, K and L). Collectively, these data indicate that the TRIM28–
364 ALKBH2 axis regulates MMS–CDDP combinatorial sensitivity and links alkylation stress to
365 cisplatin response in NSCLC.

366 **DISCUSSION**

367 Building on our previous work identifying the deubiquitinase OTUD4 as a stabilizer of an AlkB-
368 family demethylase (*2*), this study identifies a TRIM28–MAGEA6 ubiquitin pathway that
369 promotes ALKBH2 degradation, thereby regulating alkylation repair function. TRIM28, together
370 with the cancer-testis antigen MAGEA6, functions as an E3 ligase complex that promotes
371 ALKBH2 K48-linked ubiquitination and proteasomal degradation (Fig. 1–3). Under basal
372 conditions, the TRIM28–MAGEA6 complex limits ALKBH2 protein level, whereas ALKBH2
373 increases TRIM28 transcription, forming a reciprocal feedback loop that maintains steady-state
374 demethylation capacity. Alkylation stress reorganizes this loop in a time-dependent manner: acute
375 MMS exposure enhances TRIM28–ALKBH2 association and promotes ALKBH2 ubiquitination
376 and degradation, whereas prolonged MMS exposure promotes TRIM28 degradation, leading to
377 ALKBH2 stabilization, while independently promoting ALKBH2 transcription. (Fig. 8).

378 This study identifies the TRIM28–MAGEA6 as an E3 ligase complex that promotes K48-
379 linked ubiquitination and degradation of ALKBH2, providing a previously uncharacterized
380 mechanism of post-translational regulation for this duplex DNA demethylase. AlkB-family
381 enzymes participate broadly in nucleic acid repair (*61*), and ubiquitin-dependent regulation has
382 been characterized primarily for RNA-modifying members such as ALKBH5 and FTO (*17, 18*),
383 whereas the pathways regulating the stability of the DNA demethylase ALKBH2, including
384 potential E3- and DUB-linked mechanisms, remain uncharacterized. In contrast to reported
385 MAGE–TRIM architectures (*62, 63*), MAGEA6 binds both TRIM28 and ALKBH2 (Fig. 3B),
386 indicating a dual-binding mode that enhances complex assembly under alkylation stress. Although
387 ALKBH2 and ALKBH3 share a conserved catalytic core, TRIM28 preferentially interacts with
388 ALKBH2 (Fig. 1I), a selectivity likely arising from ALKBH2-specific structural features,
389 including the finger motif and long-loop region involved in duplex DNA binding (*48*). Docking
390 analysis maps the TRIM28-binding interface proximal to the DNA-binding region of ALKBH2
391 (Fig. 1J), where ssDNA competitively reduces TRIM28–ALKBH2 association (Fig. 1K),
392 suggesting that DNA engagement transiently restricts TRIM28 access during repair and permits

393 catalytic turnover before ubiquitin-dependent regulation. Notably, ALKBH2 increased TRIM28
394 mRNA and protein levels (Fig. 2, J to L), forming the transcriptional arm of this reciprocal loop,
395 consistent with evidence that ALKBH2 modulates promoter methylation and the transcription of
396 targets such as MGMT and BMI1 (*64, 65*). In conjunction with evidence that the deubiquitinase
397 OTUD4 interacts with ALKBH2 and ALKBH3 (*2*), these results indicate that AlkB-family
398 enzymes function within a broader ubiquitin-regulated network, in which the TRIM28–MAGEA6
399 complex contributes to demethylase homeostasis under both basal and stress conditions.

400 TRIM28 itself undergoes alkylation stress–dependent K48-linked ubiquitination and
401 proteasomal degradation, introducing an additional layer of regulation within the TRIM28–
402 ALKBH2 pathway. Notably, MMS selectively induced K48-linked polyubiquitination and
403 proteasomal degradation of TRIM28 (Fig. 5, A to G), whereas other genotoxic agents, including
404 TMZ, CDDP, and H_2O_2, failed to induce detectable TRIM28 degradation (Fig. 5H and fig. S5, D
405 to F). These agents modulated ALKBH2 protein levels through TRIM28-independent mechanisms:
406 H_2O_2 reduced ALKBH2 levels, and CDDP exerted minimal effects. In contrast, TMZ increased
407 ALKBH2 levels via transcriptional induction, consistent with previous observations in
408 glioblastoma cells (*10*). Mechanistically, MMS-induced TRIM28 ubiquitination and degradation
409 were attenuated by mutation of the SUMO-site mutant K554/779/804R (Fig. 5I), suggesting that
410 this lysine cluster contributes to TRIM28 modification under alkylation stress, potentially via
411 SUMO-dependent regulation and/or as candidate ubiquitin-acceptor sites. Under alkylation stress,
412 TRIM24 functioned as an upstream E3 ligase, promoting TRIM28 ubiquitination and degradation
413 (Fig. 5, J to M, S5, H to I), thereby reversing the previously described relationship in which
414 TRIM28 stabilizes TRIM24 (*66, 67*). This MMS-specific pathway is mechanistically distinct from
415 RNF4-mediated TRIM28 sumoylation and degradation during double-strand break repair (*44*) and
416 is consistent with lesion- and cue-specific organization of repair pathways and repair-complex
417 recruitment (*68, 69*). Collectively, these results indicate that alkylation stress activates a
418 coordinated ubiquitin-dependent regulatory program that targets both ALKBH2 and its E3 ligase,
419 TRIM28, thereby introducing an additional layer of regulation that modulates the TRIM28–

420 ALKBH2 axis under alkylating conditions.

421 A key mechanistic insight from this study is a time-dependent TRIM28–ALKBH2 feedback
422 loop that modulates DNA repair capacity during alkylation stress. TRIM28 promotes K48-linked
423 ubiquitination and proteasomal degradation of ALKBH2, whereas ALKBH2 increases TRIM28
424 expression at both mRNA and protein levels (Fig. 2, J to L), forming a regulatory loop that
425 maintains repair homeostasis. Acute MMS exposure enhances TRIM28–ALKBH2 association and
426 promotes ALKBH2 ubiquitination and degradation, transiently limiting repair capacity (Fig. 4).
427 During prolonged MMS exposure, progressive TRIM28 loss is accompanied by ALKBH2
428 stabilization, while MMS independently induces transcriptional upregulation of ALKBH2 (Fig. 4
429 and 5), redirecting the loop toward higher ALKBH2 availability and repair capacity. This biphasic
430 behavior parallels time-delayed feedback in the ATM–KAP1 (TRIM28) and p53–MDM2 circuits
431 that coordinate DNA repair signaling with checkpoint recovery (*70-72*). Mechanistically distinct
432 from these pathways, the TRIM28–ALKBH2 module integrates ubiquitin-mediated regulation
433 with transcriptional feedback, enabling a homeostatic reset in which ALKBH2 restores TRIM28
434 levels, thereby limiting sustained ALKBH2 accumulation.

435 Clinically, ALKBH2 is frequently elevated in lung adenocarcinoma and associates with worse
436 overall survival (Fig. 6, A to D), consistent with its role in removing alkylation lesions, thereby
437 promoting tumor cell survival under genotoxic stress (*24, 73*). Notably, TRIM28 expression is
438 associated with overall survival only in chemotherapy-treated patients, for whom higher TRIM28
439 levels are associated with worse overall survival (fig. S7, A to C), consistent with a treatment-
440 dependent prognostic association. Somatic MAGEA6 variations are enriched among smokers (fig.
441 S6C) and may further modulate this regulatory loop by altering the E3 activity of the TRIM28–
442 MAGEA6 ubiquitin module. Given that tobacco exposure increases the endogenous burden of
443 alkylation lesions (*74*), MAGEA6 variations may attenuate the activity of the TRIM28–MAGEA6
444 module and contribute to interpatient variability in alkylation repair capacity and chemoresistance.

445 Functionally, TRIM28 sensitizes cells to MMS by promoting ALKBH2 degradation, and
446 ALKBH2 re-expression reverses this effect (Fig. 6, F to I), indicating that ALKBH2 mediates the

447 MMS-sensitizing effect of TRIM28. MMS–CDDP co-treatment increased DNA damage and
448 reduced clonogenic survival, consistent with weakened ALKBH2-dependent alkylation tolerance
449 (Fig. 7, D to K). In ALKBH2-overexpressing cells, CDDP substantially reduced ALKBH2-
450 mediated protection, resulting in MMS sensitivity comparable to that observed upon ALKBH2
451 knockdown (Fig. 7E). Although TRIM28 has been linked to NSCLC chemoresistance through
452 *miR*-125b-5p/CREB1 or E2F1 signaling (*75-79*), the present data position TRIM28 upstream of
453 ALKBH2 degradation under alkylation stress. This context dependence is consistent with
454 differences in lesion chemistry and stress signaling between alkylating agents and platinum
455 crosslinkers, suggesting that the type and duration of genotoxic stress can differentially regulate
456 TRIM28 activity. These results support a model (Fig. 8) in which a time-dependent TRIM28–
457 ALKBH2 loop links alkylation stress to ubiquitin signaling and ALKBH2 availability, providing
458 a conceptual framework for combination strategies in which alkylation-associated ALKBH2
459 induction promotes tolerance that can be counteracted by agents inducing distinct DNA lesions,
460 such as platinum-based crosslinks.

461 In summary, this study identifies a stress-dependent TRIM28–ALKBH2 feedback loop that
462 regulates alkylation repair in NSCLC cells. The TRIM28–MAGEA6 E3 complex promotes K48-
463 linked polyubiquitination and proteasomal degradation of ALKBH2, while ALKBH2, in turn,
464 enhances TRIM28 expression at the mRNA and protein levels, thereby maintaining repair
465 homeostasis. Under alkylation stress, this feedback loop undergoes temporal reorganization,
466 shifting from acute TRIM28-dependent ALKBH2 degradation to prolonged TRIM28 loss,
467 accompanied by ALKBH2 stabilization and transcriptional upregulation. This stress-responsive
468 feedback loop links ubiquitin-mediated control with transcription-associated regulation to
469 coordinate cellular responses to alkylating agents. The upstream cues that trigger TRIM28
470 degradation, and the mechanisms by which they interface with transcriptional programs, remain
471 to be defined. Future studies in patient-derived and *in vivo* models are needed to clarify these
472 regulatory mechanisms and determine their relevance to chemoresistance in NSCLC.

473 **Methods**

474 **Cell culture**

475 HEK293T cells (ATCC CRL-11268, USA) and the non–small cell lung cancer (NSCLC) cell lines
476 H1299 (SCSP-589, Cell Bank of the Chinese Academy of Sciences, China), A549 (SCSP-503,
477 Cell Bank of the Chinese Academy of Sciences, China), and NCI-H460 (SCSP-584, Cell Bank of
478 the Chinese Academy of Sciences, China) were maintained in Dulbecco's modified Eagle's
479 medium (DMEM; C11995500BT, Gibco, USA) supplemented with 10% heat-inactivated fetal
480 bovine serum (FBS; 10099-141C, Gibco, USA) and penicillin–streptomycin. Cells were cultured
481 at 37 °C in a humidified 5% CO_2 incubator, and all experiments were performed using low-passage
482 cells (passages 5–15). All cell lines were routinely confirmed to be mycoplasma-free using a
483 luminescence-based detection assay (C0297, Beyotime, China).

484

485 **Plasmid constructs, mutagenesis, and viral infection**

486 Full-length human TRIM28 and ALKBH2 cDNAs were used as templates for PCR-based site-
487 directed mutagenesis. TRIM28 deletion and point mutants, including the BCC fragment (residues
488 141–400) and the RING-inactive C65/68A mutant, were generated by PCR, cloned into pENTR-
489 4, and transferred into pHAGE-CMV-Flag/HA/His via Gateway™ LR recombination (11791020,
490 Invitrogen, USA). ALKBH2 variants were cloned into pCMV-Flag for mammalian expression and
491 into pET28a-His-2×Flag for bacterial expression. All constructs were verified by Sanger
492 sequencing. Wild-type MAGEA6 cDNA was generated by reverse transcription of total RNA from
493 A549 cells, and H1299-derived MAGEA6 variants were generated analogously. Transient
494 transfections were performed using Lipo8000 (C0533, Beyotime, China).

495 Lentiviruses were produced in HEK293T cells by co-transfecting pLKO.1 or pHAGE vectors
496 with the packaging plasmids psPAX2 and pMD2.G. Viral supernatants were collected 48–72 h
497 post-transfection, clarified, and passed through 0.45-μm filters. Target cells were infected in the
498 presence of polybrene (6 μg/mL) for 12 h. Stable cell lines were selected with puromycin (1 μg/mL)

499 or blasticidin (5 μg/mL) for 3 days and maintained under selection-free conditions unless
500 otherwise indicated.
501
502 **Immunoprecipitation and western blotting**
503 For overexpression immunoprecipitation (IP), HEK293T cells were transfected with the indicated
504 plasmids using Lipo8000 and cultured for 48–72 h before lysis. Cells were lysed in a buffer
505 containing 150 mM NaCl, 50 mM Tris-HCl (pH 7.9), 1% Triton X-100, 10% glycerol, and 2 mM
506 DTT, supplemented with protease and phosphatase inhibitors. Clarified lysates were incubated
507 overnight at 4 °C with anti-Flag M2-agarose beads (A2220, Sigma-Aldrich, USA) or anti-HA-
508 agarose beads (B26201, Selleck, China). For denaturing IP, lysates were boiled in TBS containing
509 1% SDS and subsequently diluted with lysis buffer to a final SDS concentration of 0.1% before
510 IP. Each co-IP experiment was performed at least twice independently, and IP samples were
511 analyzed by western blotting (WB) two to three times with consistent results.
512 For endogenous IP in H1299 cells, lysates were prepared using the same buffer and cleared
513 by centrifugation (15,000 × *g*, 10 min, 4 °C). Supernatants were pre-cleared with Protein A/G
514 magnetic beads (B23202, Selleck, China) for 1 h and incubated overnight at 4 °C with anti-
515 TRIM28 antibody (1.5 μg). Immune complexes were captured with Protein A/G magnetic beads,
516 washed with lysis buffer, and eluted in Laemmli sample buffer. Input and flow-through fractions
517 were analyzed in parallel by WB to verify expression and loading.
518 For ssDNA competition assays, purified Flag-ALKBH2 was added to HEK293T whole-cell
519 lysates supplemented with synthetic single-stranded DNA (ssDNA) oligonucleotides and
520 incubated overnight at 4 °C. Disruption of the TRIM28–ALKBH2 interaction was assessed by
521 Flag IP followed by WB.
522 For WB, proteins were separated by SDS–PAGE and transferred to PVDF membranes.
523 Membranes were blocked with 5% non-fat milk in TBST for 1 h at room temperature, incubated
524 with primary antibodies overnight at 4 °C, and then with HRP-conjugated secondary antibodies

525 for 1–1.5 h at room temperature. Signals were detected using enhanced chemiluminescence (ECL).
526 Information on antibodies used in this study is provided in table S5.
527
528 **shRNA and CRISPR/Cas9 knockdown/knockout**
529 For shRNA-mediated knockdown, annealed oligonucleotides encoding target-specific sequences
530 were cloned into the pLKO.1 vector (8453, Addgene, USA) and packaged into lentiviral particles
531 using HEK293T cells. Target cells were transduced and selected with puromycin for 3 days to
532 establish stable knockdown lines. Knockdown efficiency was confirmed by WB. A non-targeting
533 shRNA was used as a control.
534 For CRISPR/Cas9-mediated knockout of TRIM28, single-guide RNAs (sgRNAs) were
535 designed according to established criteria and cloned into the lentiCRISPRv2 vector (52961,
536 Addgene, USA). Lentiviral particles were produced in HEK293T cells and used to transduce target
537 cells, followed by puromycin selection. Single-cell clones were isolated by limiting dilution and
538 expanded in 96-well plates, and successful knockout was verified by WB. All oligonucleotide
539 sequences are listed in table S3.
540
541 ***In vitro* MBP pull-down assay**
542 Recombinant MBP-tagged TRIM28 (MBP-TRIM28), MBP-MAGEA6, His-Flag-tagged
543 ALKBH2 (His-Flag-ALKBH2), and MBP alone were expressed in *E. coli* Rosetta (DE3). Protein
544 expression was induced with IPTG, and bacterial pellets were collected, lysed, and purified on
545 amylose resin.
546 For pull-down assays, purified MBP-TRIM28, MBP-MAGEA6, or MBP alone was
547 immobilized on amylose resin (E8021S, NEB, USA) and washed with binding buffer. The resin
548 was incubated with purified His-Flag-ALKBH2 at 4 °C with gentle mixing. After thorough
549 washing, bound proteins were eluted in Laemmli sample buffer at 95 °C and analyzed by WB
550 using anti-His or anti-Flag antibodies.
551

552 **Immunofluorescence (IF)**

553 Cells grown on glass coverslips were treated as indicated, fixed in 4% paraformaldehyde (P0099,
554 Beyotime, China) for 30 min, and permeabilized with 0.5% Triton X-100 in PBS for 15 min at
555 room temperature. After washing in PBS containing 0.1% Tween-20 (PBST), samples were
556 incubated with primary antibodies overnight at 4 °C. The next day, coverslips were washed and
557 incubated with fluorophore-conjugated secondary antibodies together with Hoechst 33342 or
558 DAPI for 1.5 h at room temperature. Coverslips were mounted and imaged using an Olympus
559 fluorescence microscope. Colocalization analysis was performed in ImageJ, and Pearson
560 correlation coefficients were calculated when applicable.

561

562 **Cycloheximide chase assay**

563 For cycloheximide (CHX) (2112, CST, USA) chase assays, cells were treated with 150 μg/mL
564 CHX for the indicated durations. Cells were harvested at each time point and analyzed by WB to
565 evaluate protein stability.

566

567 **RNA isolation and qRT-PCR**

568 Total RNA was isolated using the RNAeasy™ RNA Isolation Kit (R0026, Beyotime, China). RNA
569 concentration and purity were assessed using a NanoDrop spectrophotometer (Thermo Fisher
570 Scientific) by measuring absorbance at 260 nm and determining the A260/A280 and A260/A230
571 ratios. First-strand cDNA was synthesized using the PrimeScript™ RT reagent Kit (RR047A,
572 Takara, Japan), and qPCR was performed using the SYBR Green qPCR mix (TSE501, Tsingke,
573 China). Gene expression was normalized to β-actin. Primer sequences are listed in table S4.

574 **Protein–protein docking and structural modeling**

575 The tertiary structures of human ALKBH2 (PDB ID: 3BTZ), ALKBH3 (PDB ID: 2NCU), and the
576 RBCC domain of TRIM28 (PDB ID: 6QAJ) were retrieved from the Protein Data Bank
577 (http://www.rcsb.org). Protein–protein docking simulations were performed using the GRAMM-
578 X web server (http://gramm.compbio.ku.edu). Predicted interfaces between TRIM28 and

579 MAGEA6 were generated using AlphaFold3 (https://alphafoldserver.com/). Docking models were
580 visualized and inspected using PyMOL (version 2.6.0a0).

581 **Mass spectrometry**

582 TRIM28 complexes from H1299 cells stably expressing TAP-TRIM28 were immunoaffinity-
583 purified using anti-Flag M2-agarose beads and eluted with Flag peptide (F3290, Sigma, USA).
584 Eluates were separated by SDS–PAGE, visualized by silver staining, and subjected to LC–MS/MS.
585 Mass spectrometry analysis was performed on an Easy-nLC 1200 system (Thermo Fisher
586 Scientific) coupled to a Dr. Maisch GmbH C18 column (75 μm × 150 mm, 3 μm). Data-dependent
587 acquisition (DDA) was carried out on a Q Exactive HF-X mass spectrometer (Thermo Fisher
588 Scientific). Peptide spectra were searched against the UniProt Homo sapiens Reference Proteome
589 (UP000005640; 81791-20230317.fasta).

590

591 **Affinity purification of K48-linked polyubiquitinated proteins (Halo-TUBE)**

592 K48-linked polyubiquitinated proteins were affinity-purified under denaturing conditions using
593 Halo-tagged tandem ubiquitin-binding entity (Halo-TUBE) beads. Briefly, cells were harvested,
594 lysed, and denatured by boiling in TBS containing 1% SDS, then diluted with lysis buffer to reduce
595 SDS to 0.1% before affinity purification. Extracts were incubated with HaloLink resin (G1915,
596 Promega, USA) pre-bound to purified Halo-TUBE protein (10 μg per sample) overnight at 4 °C
597 with rotation. The resin was washed five times with washing buffer, and bound proteins were
598 eluted by boiling in Laemmli sample buffer and analyzed by WB.

599

600 **Cell proliferation, CDDP sensitivity, and synergy assays**

601 For the methyl methanesulfonate (MMS; 129925, Sigma, USA) sensitivity assay, cells (2,000–
602 5,000 cells per well in 96-well plates) were exposed to high-dose MMS (200–800 μM) for 1 h at
603 37 °C, followed by replacement with fresh medium, or were continuously treated with low-dose
604 MMS (0–200 μM) for 48 h. Cell viability was measured at 48 h using the CCK-8 assay (K1018,
605 ApexBio, USA).

606 For the cisplatin (CDDP) sensitivity assay, cells were treated with CDDP (0–40 μM) (HY-
607 17394, MCE, USA) for 48 h, and viability was assessed using the CCK-8 assay. Half-maximal
608 inhibitory concentration (IC_{50}) values were calculated using GraphPad Prism.
609 For the synergy assay, cells were treated with CDDP alone or in combination with low-dose
610 MMS for 48 h, and viability was quantified using the CCK-8 assay.
611

612 **Colony formation assay**

613 For clonogenic assays, H460 cells were seeded in 24-well plates (400 cells per well) and allowed
614 to adhere overnight. The following day, cells were treated with DMSO (vehicle control) or with
615 MMS at the indicated concentrations. For combination treatment, the medium was replaced after
616 48 h of MMS alone, CDDP alone, or MMS–CDDP co-treatment. Cells were then cultured for 5–
617 10 days to allow colony formation, fixed in 4% paraformaldehyde for 10 min, stained with 0.1%
618 crystal violet (C0121, Beyotime, China), washed, air-dried, and counted.

619 **Alkaline comet assay**

620 Alkaline single-cell gel electrophoresis (comet) assays were performed using a Comet Assay Kit
621 (KGA1302, Keygentec, China) according to the manufacturer's instructions. Comet images were
622 captured using an Olympus fluorescence microscope. Tail DNA% and tail moment were
623 quantified in ImageJ (version 1.54K) using the Comet Assay plugin. Tail DNA% was calculated
624 as: Tail DNA% = [Tail DNA intensity / (Tail DNA intensity + Head DNA intensity)] × 100%; tail
625 moment was calculated as: tail moment = tail length × Tail DNA%.

626 **3D tumorsphere culture**

627 H1299 (~2,000 cells per drop) were cultured as hanging drops for 72 h to allow spheroid formation,
628 then transferred to ultra-low-attachment (ULA) 96-well plates (LV-ULA002-96UW, Liver
629 Biotech, China). Tumor spheroids were treated with MMS and/or CDDP at the indicated
630 concentrations for 48 h. After treatment, the medium was replaced with fresh culture medium, and
631 spheroids were maintained for 3–4 weeks. Viability and cytotoxicity were assessed using a

632 Calcein-AM/propidium iodide (PI) Live/Dead assay kit (C2015S, Beyotime, China). Live (green)
633 and dead (red) fluorescence was imaged using an Olympus fluorescence microscope.

634 **Bioinformatics and clinical data analysis**

635 Clinical information for TCGA LUAD and LUSC patients was obtained from the TCGA data
636 portal (https://portal.gdc.cancer.gov/). Gene expression profiles from TCGA and protein
637 expression data from CPTAC were analyzed using UALCAN (http://ualcan.path.uab.edu/).
638 Survival analyses were performed using the Kaplan–Meier Plotter (http://kmplot.com/analysis)
639 under default settings, and hazard ratios and log-rank p-values were reported. ALKBH2
640 immunohistochemistry (IHC) images were obtained from the Human Protein Atlas
641 (http://www.proteinatlas.org). MAGEA6 and MAGEA3 variant data were examined using
642 COSMIC (http://cancer.sanger.ac.uk/cosmic) and cBioPortal (http://www.cbioportal.org). Cutoffs
643 and covariates used in each analysis are provided in the corresponding figure legends.

644 **Statistics and reproducibility**

645 All statistical analyses were performed using GraphPad Prism (version 9.5.0). Data are presented
646 as mean ± standard deviation (SD). All experiments were independently repeated at least two or
647 three times with similar results, as specified in the figure legends. Two-group comparisons were
648 performed using two-tailed unpaired Student's t-tests, unless otherwise indicated, and Mann–
649 Whitney tests were applied to nonparametric datasets. Log-rank tests were used for survival
650 analyses, and Pearson correlation coefficients (PCCs) were calculated for colocalization analyses.
651 IC_{50} values were derived using four-parameter logistic regression. Fisher's exact test was used to
652 assess differences in MAGEA3/6 variant frequencies. Exact sample sizes, numbers of independent
653 experiments, and statistical tests are provided in the figure legends.
654

655 **Data availability**

656 The data supporting the findings of this study are available within the Article and its
657 Supplementary Information.

Acknowledgments

This work was supported by the National Natural Science Foundation of China (grant no. 31971232) and the Natural Science Foundation of Hunan Province (grant no. 2019JJ40185) to YZ.

Author contributions

Conceptualization: YZ. Methodology: ZS, YD, YZ. Investigation: ZS, YD, YL, LHW, LYZ, XRF, LM, YS, BC, YH, YL. Data curation: ZS, YD, LYZ, XRF, LM. Formal analysis: YD, ZHL, JBL. Visualization: ZS, ZHL, JBL, YZ. Writing—original draft: ZS. Writing—review & editing: YZ. Supervision: YZ. Funding acquisition: YZ.

Competing interests

The authors declare no competing interests.

670 **References**

671 1. D. Fu, J. A. Calvo, L. D. Samson, Balancing repair and tolerance of DNA damage caused by alkylating agents.
672 *Nature reviews. Cancer* **12**, 104-120 (2012).
673 2. Y. Zhao, M. C. Majid, J. M. Soll, J. R. Brickner, S. Dango, N. Mosammaparast, Noncanonical regulation of
674 alkylation damage resistance by the OTUD4 deubiquitinase. *The EMBO journal* **34**, 1687-1703 (2015).
675 3. J. M. Soll, R. W. Sobol, N. Mosammaparast, Regulation of DNA Alkylation Damage Repair: Lessons and
676 Therapeutic Opportunities. *Trends in biochemical sciences* **42**, 206-218 (2017).
677 4. J. Li, X. Feng, Z. Liu, Y. Deng, Z. Sun, B. Chen, L. Wu, X. Wang, L. Miao, L. Zeng, L. Hu, Y. He, Y. Sheng,
678 Y. Liu, Y. Zhao, USP7 promotes temozolomide resistance by stabilizing MGMT in glioblastoma. *Cell death*
679 *& disease* **16**, 631 (2025).
680 5. J. A. Kloeber, Z. Lou, Critical DNA damaging pathways in tumorigenesis. *Seminars in cancer biology* **85**,
681 164-184 (2022).
682 6. S. C. Trewick, T. F. Henshaw, R. P. Hausinger, T. Lindahl, B. Sedgwick, Oxidative demethylation by
683 Escherichia coli AlkB directly reverts DNA base damage. *Nature* **419**, 174-178 (2002).
684 7. I. Leiros, M. P. Nabong, K. Grøsvik, J. Ringvoll, G. T. Haugland, L. Uldal, K. Reite, I. K. Olsbu, I.
685 Knaevelsrud, E. Moe, O. A. Andersen, N. K. Birkeland, P. Ruoff, A. Klungland, S. Bjelland, Structural basis
686 for enzymatic excision of N1-methyladenine and N3-methylcytosine from DNA. *The EMBO journal* **26**,
687 2206-2217 (2007).
688 8. C. Yi, C. He, DNA repair by reversal of DNA damage. *Cold Spring Harbor perspectives in biology* **5**,
689 a012575 (2013).
690 9. Z. Chen, Y. Zhou, C. Xue, L. Zeng, S. Deng, Z. Xu, M. Li, H. Zhao, X. He, S. Liu, J. Liu, S. Liu, S. Zhao, S.
691 Zhang, X. Peng, X. Wu, R. Bai, L. Zhuang, S. Wu, J. Zhang, D. Lin, X. Huang, J. Zheng, Psychological
692 stress-induced ALKBH5 deficiency promotes tumour innervation and pancreatic cancer via extracellular
693 vesicle transfer of RNA. *Nat Cell Biol* **27**, 1035-1047 (2025).
694 10. T. C. Johannessen, L. Prestegarden, A. Grudic, M. E. Hegi, B. B. Tysnes, R. Bjerkvig, The DNA repair protein
695 ALKBH2 mediates temozolomide resistance in human glioblastoma cells. *Neuro Oncol* **15**, 269-278 (2013).
696 11. Y. Wada, T. Naito, T. Fukushima, M. Saito, Evaluation of ALKBH2 and ALKBH3 gene regulation in patients
697 with adult T-cell leukemia/lymphoma. *Virology journal* **21**, 316 (2024).
698 12. J. A. Purslow, T. T. Nguyen, B. Khatiwada, A. Singh, V. Venditti, N (6)-methyladenosine binding induces a
699 metal-centered rearrangement that activates the human RNA demethylase Alkbh5. *Science advances* **7**,
700 (2021).
701 13. W. Dai, R. Tian, L. Yu, S. Bian, Y. Chen, B. Yin, Y. Luan, S. Chen, Z. Fan, R. Yan, X. Pan, Y. Hou, R. Li, J.
702 Chen, M. Shu, Overcoming therapeutic resistance in oncolytic herpes virotherapy by targeting IGF2BP3-
703 induced NETosis in malignant glioma. *Nature communications* **15**, 131 (2024).
704 14. Y. H. Cui, J. Wei, H. Fan, W. Li, L. Zhao, E. Wilkinson, J. Peterson, L. Xie, Z. Zou, S. Yang, M. A. Applebaum,
705 J. Kline, J. Chen, C. He, Y. Y. He, Targeting DTX2/UFD1-mediated FTO degradation to regulate antitumor
706 immunity. *Proceedings of the National Academy of Sciences of the United States of America* **121**,
707 e2407910121 (2024).
708 15. W. Liu, D. Zheng, X. Huang, Z. Wei, Z. Wei, W. Guo, TRIM17 promotes the progression of osteosarcoma
709 by regulating PDK1 m6A modification-mediated AKT/mTOR pathway activation through ubiquitination of
710 FTO. *Cell death & disease* **16**, 767 (2025).

711 16. T. Han, W. Tong, J. Xie, X. Guo, L. Zhang, FOXF2 suppressed esophageal squamous cell carcinoma by
712 reducing M2 TAMs via modulating RNF144A-FTO axis. *International immunopharmacology* **143**, 113422
713 (2024).
714 17. L. Zhang, M. Liu, Y. Xie, B. F. Yuan, Z. Peng, J. Xiong, X. L. Zhang, FTO O-GlcNAcylation promotes
715 TRIM21-mediated FTO ubiquitination degradation to sustain the negative feedback control of macrophage
716 inflammation. *Front Immunol* **16**, 1593243 (2025).
717 18. S. Meng, H. Liu, J. Xu, C. Deng, X. Qian, S. Chu, W. G. Zhu, J. Zhu, H. Yong, Z. Li, J. Bai, PRMT5-Mediated
718 ALKBH5 Methylation Promotes Colorectal Cancer Immune Evasion via Increasing CD276 Expression.
719 *Research (Washington, D.C.)* **8**, 0549 (2025).
720 19. K. Wang, F. Liu, B. Muchu, J. Deng, J. Peng, Y. Xu, F. Li, M. Ouyang, E3 ubiquitin ligase RNF180 mediates
721 the ALKBH5/SMARCA5 axis to promote colon inflammation and Th17/Treg imbalance in ulcerative colitis
722 mice. *Archives of pharmacal research* **47**, 645-658 (2024).
723 20. K. Lin, E. Zhou, T. Shi, S. Zhang, J. Zhang, Z. Zheng, Y. Pan, W. Gao, Y. Yu, m6A eraser FTO impairs
724 gemcitabine resistance in pancreatic cancer through influencing NEDD4 mRNA stability by regulating the
725 PTEN/PI3K/AKT pathway. *J Exp Clin Cancer Res* **42**, 217 (2023).
726 21. M. Song, F. Yi, F. Zeng, L. Zheng, L. Huang, X. Sun, Q. Huang, J. Deng, H. Wang, W. Gu, USP18 Stabilized
727 FTO Protein to Activate Mitophagy in Ischemic Stroke Through Repressing m6A Modification of SIRT6.
728 *Molecular neurobiology* **61**, 6658-6674 (2024).
729 22. X. Zhou, Q. Xia, B. Wang, J. Li, B. Liu, S. Wang, M. Huang, R. Zhong, S. Y. Cheng, X. Wang, X. Jiang, T.
730 Huang, USP14 modulates stem-like properties, tumorigenicity, and radiotherapy resistance in glioblastoma
731 stem cells through stabilization of MST4-phosphorylated ALKBH5. *Theranostics* **15**, 2293-2314 (2025).
732 23. G. Chang, G. S. Xie, L. Ma, P. Li, L. Li, H. T. Richard, USP36 promotes tumorigenesis and drug sensitivity
733 of glioblastoma by deubiquitinating and stabilizing ALKBH5. *Neuro Oncol* **25**, 841-853 (2023).
734 24. T. Duncan, S. C. Trewick, P. Koivisto, P. A. Bates, T. Lindahl, B. Sedgwick, Reversal of DNA alkylation
735 damage by two human dioxygenases. *Proceedings of the National Academy of Sciences of the United States*
736 *of America* **99**, 16660-16665 (2002).
737 25. J. Ringvoll, L. M. Nordstrand, C. B. Vågbø, V. Talstad, K. Reite, P. A. Aas, K. H. Lauritzen, N. B. Liabakk,
738 A. Bjørk, R. W. Doughty, P. Falnes, H. E. Krokan, A. Klungland, Repair deficient mice reveal mABH2 as
739 the primary oxidative demethylase for repairing 1meA and 3meC lesions in DNA. *The EMBO journal* **25**,
740 2189-2198 (2006).
741 26. P. Wang, J. Wu, S. Ma, L. Zhang, J. Yao, K. A. Hoadley, M. D. Wilkerson, C. M. Perou, K. L. Guan, D. Ye,
742 Y. Xiong, Oncometabolite D-2-Hydroxyglutarate Inhibits ALKBH DNA Repair Enzymes and Sensitizes IDH
743 Mutant Cells to Alkylating Agents. *Cell reports* **13**, 2353-2361 (2015).
744 27. Q. Li, Y. Huang, X. Liu, J. Gan, H. Chen, C. G. Yang, Rhein Inhibits AlkB Repair Enzymes and Sensitizes
745 Cells to Methylated DNA Damage. *J Biol Chem* **291**, 11083-11093 (2016).
746 28. G. Wu, Y. Yan, Y. Cai, B. Peng, J. Li, J. Huang, Z. Xu, J. Zhou, ALKBH1-8 and FTO: Potential Therapeutic
747 Targets and Prognostic Biomarkers in Lung Adenocarcinoma Pathogenesis. *Frontiers in cell and*
748 *developmental biology* **9**, 633927 (2021).
749 29. S. S. Wu, W. Xu, S. Liu, B. Chen, X. L. Wang, Y. Wang, S. F. Liu, J. Q. Wu, Down-regulation of ALKBH2
750 increases cisplatin sensitivity in H1299 lung cancer cells. *Acta pharmacologica Sinica* **32**, 393-398 (2011).
751 30. J. Chen, X. Wang, Y. Yuan, H. Chen, L. Zhang, H. Xiao, J. Chen, Y. Zhao, J. Chang, W. Guo, X. J. Liang,

752 Exploiting the acquired vulnerability of cisplatin-resistant tumors with a hypoxia-amplifying DNA repair-
753 inhibiting (HYDRI) nanomedicine. *Science advances* **7**, (2021).
754 31. X. Li, H. Zeng, L. Zhang, J. Zhang, Y. Guo, J. Leng, An integrated LC-MS/MS platform for noninvasive
755 urinary nucleus acid adductomics: A pilot study for tobacco exposure. *Journal of hazardous materials* **474**,
756 134780 (2024).
757 32. M. E. Hegi, A. C. Diserens, T. Gorlia, M. F. Hamou, N. de Tribolet, M. Weller, J. M. Kros, J. A. Hainfellner,
758 W. Mason, L. Mariani, J. E. Bromberg, P. Hau, R. O. Mirimanoff, J. G. Cairncross, R. C. Janzer, R. Stupp,
759 MGMT gene silencing and benefit from temozolomide in glioblastoma. *The New England journal of*
760 *medicine* **352**, 997-1003 (2005).
761 33. D. L. Wilson, A. A. Beharry, A. Srivastava, T. R. O'Connor, E. T. Kool, Fluorescence Probes for ALKBH2
762 Allow the Measurement of DNA Alkylation Repair and Drug Resistance Responses. *Angewandte Chemie*
763 *(International ed. in English)* **57**, 12896-12900 (2018).
764 34. J. R. Brickner, J. M. Soll, P. M. Lombardi, C. B. Vagbo, M. C. Mudge, C. Oyeniran, R. Rabe, J. Jackson, M.
765 E. Sullender, E. Blazosky, A. K. Byrum, Y. Zhao, M. A. Corbett, J. Gecz, M. Field, A. Vindigni, G. Slupphaug,
766 C. Wolberger, N. Mosammaparast, A ubiquitin-dependent signalling axis specific for ALKBH-mediated
767 DNA dealkylation repair. *Nature* **551**, 389-393 (2017).
768 35. S. Hatakeyama, TRIM proteins and cancer. *Nat Rev Cancer* **11**, 792-804 (2011).
769 36. J. Dudley-Fraser, D. Esposito, K. A. McPhie, C. Morley-Williams, T. Auchynnikava, K. Rittinger,
770 Identification of RING E3 pseudoligases in the TRIM protein family. *Nature communications* **16**, 3456
771 (2025).
772 37. P. Czerwińska, S. Mazurek, M. Wiznerowicz, The complexity of TRIM28 contribution to cancer. *Journal of*
773 *biomedical science* **24**, 63 (2017).
774 38. W. Zhang, M. Tang, L. Wang, H. Zhou, J. Gao, Z. Chen, B. Zhao, P. Zheng, Lnc956-TRIM28-HSP90B1
775 complex on replication forks promotes CMG helicase retention to ensure stem cell genomic stability and
776 embryogenesis. *Science advances* **9**, eadf6277 (2023).
777 39. Z. Yalçin, S. Y. Lam, M. H. Peuscher, J. van der Torre, S. Zhu, P. V. Iyengar, D. Salas-Lloret, I. de Krijger,
778 N. Moatti, R. van der Lugt, M. Falcone, A. Cerutti, O. B. Bleijerveld, L. Hoekman, R. González-Prieto, J. J.
779 L. Jacobs, UBE2D3 facilitates NHEJ by orchestrating ATM signalling through multi-level control of RNF168.
780 *Nature communications* **15**, 5032 (2024).
781 40. A. A. Goodarzi, T. Kurka, P. A. Jeggo, KAP-1 phosphorylation regulates CHD3 nucleosome remodeling
782 during the DNA double-strand break response. *Nature structural & molecular biology* **18**, 831-839 (2011).
783 41. Y. Li, H. Xie, S. Liu, Z. Ruan, B. Wang, Resveratrol Alleviates Ischemia-Reperfusion-Induced Neuronal
784 Damage by Inhibiting NR3C2-Mediated TRIM28 Expression. *Journal of integrative neuroscience* **24**, 31375
785 (2025).
786 42. Z. Wang, A. Mierxiati, W. Zhu, T. Li, H. Xu, F. Wan, D. Ye, FOXA1-dependent NSUN2 facilitates the
787 advancement of prostate cancer by preserving TRIM28 mRNA stability in a m5C-dependent manner. *NPJ*
788 *precision oncology* **9**, 127 (2025).
789 43. S. Jana, M. Mondal, S. Mahale, B. Gupta, K. R. Prasasvi, L. Kandasami, N. Jha, A. Chowdhury, V. Santosh,
790 C. Kanduri, K. Somasundaram, PITAR, a DNA damage-inducible cancer/testis long noncoding RNA,
791 inactivates p53 by binding and stabilizing TRIM28 mRNA. *eLife* **12**, (2024).
792 44. C. Y. Kuo, X. Li, X. Q. Kong, C. Luo, C. C. Chang, Y. Chung, H. M. Shih, K. K. Li, D. K. Ann, An arginine-

793 rich motif of ring finger protein 4 (RNF4) oversees the recruitment and degradation of the phosphorylated
794 and SUMOylated Krüppel-associated box domain-associated protein 1 (KAP1)/TRIM28 protein during
795 genotoxic stress. *J Biol Chem* **289**, 20757-20772 (2014).
796 45. Y. Chen, W. Pang, G. Ma, Y. Yan, Z. Xiao, Y. Chen, Z. Ding, L. Chen, X. Hou, H. Cao, March5-mediated
797 Trim28 degradation preserves islet β-cell function in mice. *Nature communications* **16**, 7073 (2025).
798 46. J. M. Doyle, J. Gao, J. Wang, M. Yang, P. R. Potts, MAGE-RING protein complexes comprise a family of
799 E3 ubiquitin ligases. *Molecular cell* **39**, 963-974 (2010).
800 47. K. Li, M. W. Krone, A. Butrin, M. J. Bond, B. M. Linhares, C. M. Crews, Development of Ligands and
801 Degraders Targeting MAGE-A3. *Journal of the American Chemical Society* **146**, 24884-24891 (2024).
802 48. C. G. Yang, C. Yi, E. M. Duguid, C. T. Sullivan, X. Jian, P. A. Rice, C. He, Crystal structures of DNA/RNA
803 repair enzymes AlkB and ABH2 bound to dsDNA. *Nature* **452**, 961-965 (2008).
804 49. H. P. Le, X. Ma, J. Vaquero, M. Brinkmeyer, F. Guo, W. D. Heyer, J. Liu, DSS1 and ssDNA regulate
805 oligomerization of BRCA2. *Nucleic acids research* **48**, 7818-7833 (2020).
806 50. P. Gu, W. Deng, M. Lei, S. Chang, Single strand DNA binding proteins 1 and 2 protect newly replicated
807 telomeres. *Cell research* **23**, 705-719 (2013).
808 51. G. Dürnberger, T. Bürckstümmer, K. Huber, R. Giambruno, T. Doerks, E. Karayel, T. R. Burkard, I. Kaupe,
809 A. C. Müller, A. Schönegger, G. F. Ecker, H. Lohninger, P. Bork, K. L. Bennett, G. Superti-Furga, J. Colinge,
810 Experimental characterization of the human non-sequence-specific nucleic acid interactome. *Genome*
811 *biology* **14**, R81 (2013).
812 52. Y. Feng, J. Gao, M. Yang, When MAGE meets RING: insights into biological functions of MAGE proteins.
813 *Protein Cell* **2**, 7-12 (2011).
814 53. C. T. Pineda, S. Ramanathan, K. Fon Tacer, J. L. Weon, M. B. Potts, Y. H. Ou, M. A. White, P. R. Potts,
815 Degradation of AMPK by a cancer-specific ubiquitin ligase. *Cell* **160**, 715-728 (2015).
816 54. Y. H. Tsang, Y. Wang, K. Kong, C. Grzeskowiak, O. Zagorodna, T. Dogruluk, H. Lu, N. Villafane, V. H.
817 Bhavana, D. Moreno, S. H. Elsea, H. Liang, G. B. Mills, K. L. Scott, Differential expression of MAGEA6
818 toggles autophagy to promote pancreatic cancer progression. *eLife* **9**, (2020).
819 55. X. Bu, X. Qu, K. Guo, X. Meng, X. Yang, Q. Huang, W. Dou, L. Feng, X. Wei, J. Gao, W. Sun, M. Chao, L.
820 Han, Y. Hu, L. Shen, J. Zhang, L. Wang, CD147 confers temozolomide resistance of glioma cells via the
821 regulation of β-TrCP/Nrf2 pathway. *International journal of biological sciences* **17**, 3013-3023 (2021).
822 56. D. B. Lombard, W. J. Kohler, A. H. Guo, C. Gendron, M. Han, W. Ding, Y. Lyu, T. T. Ching, F. Y. Wang, T.
823 S. Chakraborty, Z. Nikolovska-Coleska, Y. Duan, T. Girke, A. L. Hsu, S. D. Pletcher, R. A. Miller, High-
824 throughput small molecule screening reveals Nrf2-dependent and -independent pathways of cellular stress
825 resistance. *Science advances* **6**, (2020).
826 57. D. H. Lee, S. G. Jin, S. Cai, Y. Chen, G. P. Pfeifer, T. R. O'Connor, Repair of methylation damage in DNA
827 and RNA by mammalian AlkB homologues. *J Biol Chem* **280**, 39448-39459 (2005).
828 58. A. V. Ivanov, H. Peng, V. Yurchenko, K. L. Yap, D. G. Negorev, D. C. Schultz, E. Psulkowski, W. J. Fredericks,
829 D. E. White, G. G. Maul, M. J. Sadofsky, M. M. Zhou, F. J. Rauscher, 3rd, PHD domain-mediated E3 ligase
830 activity directs intramolecular sumoylation of an adjacent bromodomain required for gene silencing.
831 *Molecular cell* **28**, 823-837 (2007).
832 59. C. Prince, G. Hammerton, A. E. Taylor, E. L. Anderson, N. J. Timpson, G. Davey Smith, M. R. Munafò, C.
833 L. Relton, R. C. Richmond, Investigating the impact of cigarette smoking behaviours on DNA methylation

patterns in adolescence. *Hum Mol Genet* **28**, 155-165 (2019).

60. H. J. Kim, J. H. Lee, S. J. Kim, G. S. Oh, H. D. Moon, K. B. Kwon, C. Park, B. H. Park, H. K. Lee, S. Y. Chung, R. Park, H. S. So, Roles of NADPH oxidases in cisplatin-induced reactive oxygen species generation and ototoxicity. *The Journal of neuroscience : the official journal of the Society for Neuroscience* **30**, 3933-3946 (2010).

61. G. L. Xu, M. Bochtler, Reversal of nucleobase methylation by dioxygenases. *Nature chemical biology* **16**, 1160-1169 (2020).

62. C. T. Pineda, P. R. Potts, Oncogenic MAGEA-TRIM28 ubiquitin ligase downregulates autophagy by ubiquitinating and degrading AMPK in cancer. *Autophagy* **11**, 844-846 (2015).

63. X. Jin, Y. Pan, L. Wang, L. Zhang, R. Ravichandran, P. R. Potts, J. Jiang, H. Wu, H. Huang, MAGE-TRIM28 complex promotes the Warburg effect and hepatocellular carcinoma progression by targeting FBP1 for degradation. *Oncogenesis* **6**, e312 (2017).

64. A. Malacrida, A. Di Domizio, A. Bentivegna, G. Cislaghi, E. Messuti, S. M. Tabano, C. Giussani, V. Zuliani, M. Rivara, G. Nicolini, MV1035 Overcomes Temozolomide Resistance in Patient-Derived Glioblastoma Stem Cell Lines. *Biology* **11**, (2022).

65. B. Ke, K. Ye, S. Cheng, ALKBH2 inhibition alleviates malignancy in colorectal cancer by regulating BMI1-mediated activation of NF-κB pathway. *World journal of surgical oncology* **18**, 328 (2020).

66. K. W. Fong, J. C. Zhao, B. Song, B. Zheng, J. Yu, TRIM28 protects TRIM24 from SPOP-mediated degradation and promotes prostate cancer progression. *Nature communications* **9**, 5007 (2018).

67. B. Herquel, K. Ouararhni, K. Khetchoumian, M. Ignat, M. Teletin, M. Mark, G. Béchade, A. Van Dorsselaer, S. Sanglier-Cianférani, A. Hamiche, F. Cammas, I. Davidson, R. Losson, Transcription cofactors TRIM24, TRIM28, and TRIM33 associate to form regulatory complexes that suppress murine hepatocellular carcinoma. *Proceedings of the National Academy of Sciences of the United States of America* **108**, 8212-8217 (2011).

68. J. R. Lin, M. K. Zeman, J. Y. Chen, M. C. Yee, K. A. Cimprich, SHPRH and HLTF act in a damage-specific manner to coordinate different forms of postreplication repair and prevent mutagenesis. *Molecular cell* **42**, 237-249 (2011).

69. N. Tsao, J. R. Brickner, R. Rodell, A. Ganguly, M. Wood, C. Oyeniran, T. Ahmad, H. Sun, A. Bacolla, L. Zhang, V. Lukinović, J. M. Soll, B. A. Townley, A. G. Casanova, J. A. Tainer, C. He, A. Vindigni, N. Reynoird, N. Mosammaparast, Aberrant RNA methylation triggers recruitment of an alkylation repair complex. *Molecular cell* **81**, 4228-4242.e4228 (2021).

70. H. Jaiswal, J. Benada, E. Müllers, K. Akopyan, K. Burdova, T. Koolmeister, T. Helleday, R. H. Medema, L. Macurek, A. Lindqvist, ATM/Wip1 activities at chromatin control Plk1 re-activation to determine G2 checkpoint duration. *The EMBO journal* **36**, 2161-2176 (2017).

71. C. Wang, A. Ivanov, L. Chen, W. J. Fredericks, E. Seto, F. J. Rauscher, 3rd, J. Chen, MDM2 interaction with nuclear corepressor KAP1 contributes to p53 inactivation. *The EMBO journal* **24**, 3279-3290 (2005).

72. Y. Zhao, M. Tan, X. Liu, X. Xiong, Y. Sun, Inactivation of ribosomal protein S27-like confers radiosensitivity via the Mdm2-p53 and Mdm2-MRN-ATM axes. *Cell death & disease* **9**, 145 (2018).

73. S. Feng, Z. Xu, J. Peng, M. Zhang, The AlkB Family: Potential Prognostic Biomarkers and Therapeutic Targets in Glioblastoma. *Frontiers in oncology* **12**, 847821 (2022).

74. T. T. Hoang, Y. Lee, D. L. McCartney, E. T. G. Kersten, C. M. Page, P. M. Hulls, M. Lee, R. M. Walker, C.

875 E. Breeze, B. D. Bennett, A. B. Burkholder, J. Ward, A. L. Brantsæter, I. H. Caspersen, A. A. Motsinger-Reif,
876 M. Richards, J. D. White, S. Zhao, R. C. Richmond, M. C. Magnus, G. H. Koppelman, K. L. Evans, R. E.
877 Marioni, S. E. Håberg, S. J. London, Comprehensive evaluation of smoking exposures and their interactions
878 on DNA methylation. *EBioMedicine* **100**, 104956 (2024).
879 75. Q. Tan, J. Ma, H. Zhang, X. Wu, Q. Li, X. Zuo, Y. Jiang, H. Liu, L. Yan, miR-125b-5p upregulation by
880 TRIM28 induces cisplatin resistance in non-small cell lung cancer through CREB1 inhibition. *BMC*
881 *pulmonary medicine* **22**, 469 (2022).
882 76. L. Liu, L. Xiao, X. Liang, L. Chen, L. Cheng, L. Zhang, X. Wu, Q. Xu, C. Ma, TRIM28 knockdown increases
883 sensitivity to etoposide by upregulating E2F1 in non-small cell lung cancer. *Oncology reports* **37**, 3597-3605
884 (2017).
885 77. L. Ginn, J. Maltas, M. J. Baker, A. Chaturvedi, L. Wilson, R. Guilbert, F. M. R. Amaral, L. Priest, H. Mole,
886 F. Blackhall, Z. Diamantopoulou, T. C. P. Somervaille, A. Hurlstone, A. Malliri, A TIAM1-TRIM28 complex
887 mediates epigenetic silencing of protocadherins to promote migration of lung cancer cells. *Proceedings of*
888 *the National Academy of Sciences of the United States of America* **120**, e2300489120 (2023).
889 78. T. Saxena, A. Quan, E. Chan, N. Kozlova, L. Matai, J. D. Lee, R. Rupaimoole, F. Beca, T. Muranen, F. J.
890 Slack, EGFR-induced lncRNA TRIDENT promotes drug resistance in non-small cell lung cancer via
891 phospho-TRIM28-mediated DNA damage repair. *Proceedings of the National Academy of Sciences of the*
892 *United States of America* **122**, e2415389122 (2025).
893 79. L. Lundholm, P. Hååg, D. Zong, T. Juntti, B. Mörk, R. Lewensohn, K. Viktorsson, Resistance to DNA-
894 damaging treatment in non-small cell lung cancer tumor-initiating cells involves reduced DNA-PK/ATM
895 activation and diminished cell cycle arrest. *Cell death & disease* **4**, e478 (2013).
896

897 **Figure legends**

898 **Figure 1. TRIM28 directly binds ALKBH2. (A)** Silver staining and LC–MS/MS identification
899 of ALKBH2 as a TRIM28-associated protein following affinity purification from H1299 NSCLC
900 cells; the TRIM28 band is indicated. **(B)** Co-immunoprecipitation (co-IP) analysis of HEK293T
901 cells co-expressing HA-ALKBH2 and Flag-TRIM28 or Flag-TRIM24; Flag IP was followed by
902 western blotting (WB). Data are representative of two independent experiments with similar
903 results. **(C)** Reciprocal co-IP using HA-ALKBH2 and Flag-TRIM28 (or HA-GFP control), HA IP
904 was followed by WB. Data are representative of two independent experiments with similar results.
905 **(D)** Schematic of full-length TRIM28 and truncation mutants. **(E)** Domain mapping using Flag IP
906 followed by WB in HEK293T cells co-transfected with HA-ALKBH2 and individual TRIM28
907 truncation constructs. Data are representative of two independent experiments. **(F)** Endogenous
908 ALKBH2–TRIM28 interaction detected by co-IP using an anti-TRIM28 antibody in H1299 cell
909 lysates. Data are representative of two independent experiments. **(G)** Immunofluorescence (IF)
910 showing nuclear co-localization of endogenous ALKBH2 (green) and TRIM28 (red); nuclei were
911 counterstained with DAPI (blue). Scale bar, 20 μm. Pearson correlation coefficient (PCC) = 0.896
912 ± 0.016 (mean ± SD, n = 42 cells). **(H)** *In vitro* MBP pull-down assay using recombinant His-Flag-
913 ALKBH2 and purified MBP-TRIM28. Data are representative of two independent experiments.
914 **(I)** Specificity profiling of endogenous TRIM28 binding in HEK293T cells transfected with Flag-
915 ALKBH2 or Flag-ALKBH3. Data are representative of two independent experiments with similar
916 results. **(J)** GRAMM-X docking of TRIM28 RBCC (cyan) with ALKBH2 (light red) or ALKBH3
917 (green). Middle panel: magnified interface highlighting the Finger and Long-loop motifs (red).
918 Right panel: superposition with the ALKBH2–DNA structure (orange), showing partial overlap
919 between TRIM28- and DNA-binding surfaces. **(K)** Flag IP of lysates from HEK293T cells
920 expressing Flag-ALKBH2 in the presence of increasing ssDNA concentrations. Data are
921 representative of two independent experiments with similar results.

922

923 **Figure 2. TRIM28 promotes K48-linked ubiquitination and proteasomal degradation of**
924 **ALKBH2. (A)** In vivo ubiquitination assay in HEK293T cells co-transfected with Flag-ALKBH2

925 and HA-ubiquitin (Ub), treated with MG132 (10 μM, 6 h). Lysates were subjected to denaturing
926 Flag IP (1% SDS) followed by WB. Data are from three independent experiments. **(B)** Denaturing
927 Flag IP followed by WB in HEK293T cells co-transfected with Flag-ALKBH2 and HA-tagged
928 WT, K48-only, or K48R ubiquitin. Data are representative of two independent experiments with
929 similar results. **(C)** K48-linked polyubiquitin enrichment using Halo-TUBE beads in HEK293T
930 cells expressing Flag-ALKBH2 treated with MG132. Data are representative of two independent
931 experiments with similar results. **(D)** Denaturing Flag IP in HEK293T cells co-transfected with
932 Flag-ALKBH2, His-TRIM28, and HA-K48-only ubiquitin. Data are representative of two
933 independent experiments with similar results. **(E)** Analysis of ALKBH2 ubiquitination in
934 HEK293T cells co-transfected with Flag-ALKBH2 and WT or RING-inactive (C65/68A) His-
935 TRIM28. Representative of two independent experiments. **(F)** Denaturing Flag IP assessing K48-
936 linked ALKBH2 ubiquitination in TRIM28-knockdown HEK293T cells reconstituted with
937 shRNA-resistant TRIM28. Representative of two independent experiments. **(G)** WB analysis of
938 H1299 and A549 cells transduced with control (shCon) or TRIM28 shRNAs. N = 3 independent
939 experiments. **(H)** qRT-PCR quantification of ALKBH2 mRNA in H1299 cells after TRIM28
940 depletion. Data points are shown as technical replicates (N = 4); experiments were independently
941 repeated twice with similar results. **(I)** WB analysis of ALKBH2 levels in H1299 and HEK293T
942 cells overexpressing graded doses of TRIM28. N = 3 independent repeats. **(J)** WB analysis of
943 H1299 cells transduced with control or ALKBH2 shRNAs. N = 3 independent experiments. **(K)**
944 WB analysis of ALKBH2-depleted H1299 cells reconstituted with Flag-ALKBH2. N = 3
945 independent repeats. **(L)** qRT-PCR of TRIM28 transcript levels in H1299 cells expressing empty
946 vector or Flag-ALKBH2 (N = 4). Data were obtained using the same replication scheme as in (H).
947 Error bars indicate mean ± SD. Statistical comparisons were performed using unpaired two-tailed
948 Student's *t*-tests; NS, not significant.
949
950 **Figure 3. MAGEA6 enhances the TRIM28–ALKBH2 interaction and promotes ALKBH2**
951 **degradation. (A)** Flag IP analysis of the interaction between Myc-MAGEA6 and Flag-ALKBH2

952 (or GFP control) in HEK293T cells. Representative of two independent experiments with similar
953 results. **(B)** *In vitro* pull-down assay using recombinant His-Flag-ALKBH2 and purified MBP-
954 MAGEA6. Representative of two independent experiments. **(C)** Flag IP in HEK293T cells (±
955 TRIM28 knockdown) co-transfected with HA-ALKBH2 and Flag-MAGEA6. Representative of
956 two independent experiments. **(D)** Flag IP analysis of the ALKBH2–TRIM28 interaction in
957 HEK293T cells transfected with Myc-MAGEA6. Representative of two independent experiments.
958 **(E)** HA IP in H1299 cells stably expressing HA-ALKBH2 following MAGEA3/6 knockdown with
959 shMAGEA3/6#1 or shMAGEA3/6#2. Representative of two independent experiments with
960 similar results. **(F)** Halo-TUBE pull-down in TRIM28-knockdown HEK293T cells overexpressing
961 Myc-MAGEA6. Representative of two independent experiments. **(G)** WB analysis of ALKBH2
962 stability in sgControl or TRIM28-knockout (sgTRIM28) H1299 cells transfected with MAGEA6
963 and treated with cycloheximide (CHX, 150 μg/mL). **(H)** Quantification of ALKBH2 protein levels
964 from (G). Data were quantified from 3 biological replicates (N = 3). **(I)** Flag IP mapping
965 interactions between Flag-MAGEA6 (WT or mutants), endogenous TRIM28, and co-expressed
966 HA-ALKBH2 in HEK293T cells. Representative of two independent experiments. **(J)** Halo-TUBE
967 pull-down of ubiquitinated proteins in HEK293T cells co-expressing HA-ALKBH2 and Flag-
968 MAGEA6 (WT or mutants). Representative of two independent experiments with similar results.
969 **(K)** Flag IP of HEK293T cells transfected with HA-ALKBH2 and cancer-associated Flag-
970 MAGEA6 mutants. Representative of two independent experiments. Error bars indicate mean ±
971 SD. Statistical comparisons were performed using unpaired two-tailed Student's *t*-tests. NS, not
972 significant.
973
974 **Figure 4. MMS dynamically regulates the TRIM28–ALKBH2 pathway. (A)** Flag IP from
975 H1299 cells expressing HA-ALKBH2 and Flag-TRIM28 treated with MMS (100 μM) and MG132
976 (10 μM) for the indicated times. Representative of two independent experiments with similar
977 results. **(B)** Flag IP from H1299 cells expressing Flag-TRIM28 treated with the indicated MMS
978 concentrations (3 h, +MG132). Representative of two independent experiments. **(C)** WB analysis

979 of MAGEA3/6 in nuclear and cytoplasmic fractions of H1299 cells treated with MMS (100 μM,
980 4 h). Representative of two independent experiments. **(D)** Flag IP of H1299 cells expressing Flag-
981 ALKBH2 treated with MMS (0–200 μM, 3 h) plus MG132. Representative of two independent
982 experiments with similar results. **(E)** Degradation assay in H1299 cells expressing TAP-ALKBH2
983 transduced with Flag-TRIM28 or vector and treated with MMS (100 μM). N = 3 independent
984 repeats. **(F)** Flag IP of cell lysates incubated with ssDNA (1 μM), H_2O_2 (200 μM), ascorbate (Vc,
985 500 μM), or EDTA (5 mM). Representative of two independent experiments with similar results.
986 **(G)** Flag IP assessing the effect of EDTA (5 mM) on H_2O_2-induced interactions in ssDNA-
987 containing lysates. Representative of two independent experiments. **(H)** Halo-TUBE pull-down in
988 H1299 cells expressing TAP-ALKBH2 treated with MG132 (10 μM), MMS (100 μM), and Vc
989 (500 μM) for 8 h. Representative of two independent experiments with similar results. **(I)** WB
990 analysis of ALKBH2 in H1299 and H460 cells treated with MMS (100 μM). **(J)** Quantification of
991 ALKBH2 protein levels from (I). Data were quantified from 4 biological replicates (N = 4). **(K)**
992 WB analysis of H1299 cells expressing HA-TRIM28 treated with MMS (100 μM). N = 3
993 independent experiments. **(L)** qRT-PCR of ALKBH2 in H1299 cells treated with MMS (100 μM).
994 Data points are shown as technical replicates (N = 4); experiments were independently repeated
995 twice with similar results. Error bars indicate mean ± SD. Statistical comparisons were performed
996 using unpaired two-tailed Student's *t*-tests.
997
998 **Figure 5. MMS induces K48-linked ubiquitination and proteasomal degradation of TRIM28.**
999 **(A, B)** WB analysis of TRIM28 levels in H1299 cells treated with MMS in a time-dependent (A)
1000 or dose-dependent (B) manner. N = 3 independent experiments. **(C)** qRT-PCR of TRIM28 mRNA
1001 in cells treated with MMS (100 μM). Data points are shown as technical replicates (N = 3);
1002 experiments were independently repeated twice with similar results. **(D)** Denaturing Flag IP of
1003 HEK293T cells expressing Flag-TRIM28 and HA-Ub treated with MMS and MG132 (10 μM).
1004 Representative of two independent experiments with similar results. **(E)** Flag IP and K48-specific
1005 ubiquitin WB in H1299 cells expressing Flag-TRIM28 treated with MMS (100 μM) + MG132.

1006 Representative of two independent experiments with similar results. **(F)** Denaturing Flag IP in
1007 HEK293T cells transfected with Flag-TRIM28 and HA-Ub (K48-only) treated with MMS (100
1008 μM). Representative of two independent experiments. **(G)** Halo-TUBE pull-down of endogenous
1009 TRIM28 in H1299 cells treated with MG132 and increasing MMS. Representative of two
1010 independent experiments. **(H)** Halo-TUBE pull-down comparing the effects of MMS (200 μM),
1011 temozolomide (TMZ, 200 μM), cisplatin (CDDP, 20 μM), or H_2O_2 (300 μM) on TRIM28
1012 ubiquitination (+MG132, 6 h). Representative of two independent experiments with similar results.
1013 **(I)** Halo-TUBE pull-down in HEK293T cells expressing Flag-TRIM28 WT or the SUMO-
1014 deficient mutant (K554/779/804R) treated with MMS. Representative of two independent
1015 experiments. **(J)** Flag IP in H1299 cells expressing Flag-TRIM28 treated with MMS (100 μM) +
1016 MG132. Representative of two independent experiments. **(K)** Flag IP in HEK293T cells
1017 expressing Flag-TRIM28 and Myc-MAGEA6 treated with MMS. Representative of two
1018 independent experiments. **(L)** Flag IP and WB in HEK293T cells expressing Flag-TRIM24 treated
1019 with MMS + MG132. Results were reproduced in independent experiments. **(M)** Halo-TUBE
1020 enrichment of K48-linked proteins in HEK293T cells overexpressing Flag-TRIM24 treated with
1021 MMS. Representative of two independent experiments with similar results. Error bars indicate
1022 mean ± SD. Statistical comparisons were performed using unpaired two-tailed Student's *t*-tests.
1023 NS, not significant.
1024
1025 **Figure 6. The TRIM28–ALKBH2 axis is clinically relevant and regulates sensitivity to**
1026 **alkylation damage. (A)** Relative mRNA expression of ALKBH2, ALKBH3, and MGMT in
1027 LUAD versus normal lung (TCGA dataset; Mann–Whitney test). **(B)** Representative ALKBH2
1028 IHC staining in LUAD and matched normal lung (Human Protein Atlas). Scale bar = 100 μm. **(C)**
1029 WB analysis of ALKBH2, TRIM28, ALKBH3, and MGMT in NSCLC cell lines and BEAS-2B
1030 cells. N = 3 independent experiments. **(D, E)** Kaplan–Meier overall survival of LUAD patients
1031 stratified by ALKBH2 (D) or ALKBH3 (E) mRNA expression. **(F)** CCK-8 proliferation assay in
1032 H1299 cells following ALKBH2 knockdown. **(G)** CCK-8 viability assay in H1299 cells with

1033 ALKBH2 knockdown, measured 48 h after a 1 h MMS pulse. **(H)** CCK-8 viability assay in H1299
1034 cells overexpressing Flag-TRIM28 WT or the RING-inactive mutant (C65/68A) after MMS pulse.
1035 **(I)** MMS sensitivity assessment in H1299 cells with TRIM28 knockdown and rescue. **(J)** Rescue
1036 of MMS hypersensitivity in H1299 cells by ALKBH2 co-expression. **(K)** Effect of MAGEA6
1037 overexpression on MMS cytotoxicity. **(L)** Effect of the TRIM28-binding–deficient MAGEA6
1038 mutant (D156E/S157Y) on MMS sensitivity. Data points are shown for panels F–L. For panels F,
1039 G, H, I, J, and L, data points represent four technical replicates from one representative experiment;
1040 the experiment was repeated twice with similar results. Panel K contains three technical replicates
1041 and was also repeated twice with similar results. Error bars indicate mean ± SD. Statistical
1042 comparisons were performed using unpaired two-tailed Student's *t*-tests or Mann–Whitney tests
1043 where appropriate. NS, not significant.
1044
1045 **Figure 7. Combining MMS with CDDP synergistically enhances cancer cell killing. (A)** CCK-
1046 8 viability assay of H1299 cells with TRIM28 knockdown treated with continuous low-dose MMS
1047 (48 h). **(B, C)** Colony formation assay of H460 cells overexpressing TRIM28 treated with MMS
1048 (100 μM) for 48 h, followed by drug removal and a 7-day growth period; representative images
1049 (B) and quantification (C). Colony numbers were averaged from 3 plates per experiment (N = 3),
1050 and the assay was repeated twice with similar results. **(D)** CCK-8 assay of H1299 cells
1051 overexpressing TRIM28 treated with MMS ± 2 μM CDDP. **(E)** CCK-8 assay of H1299 cells with
1052 ALKBH2 knockdown rescued by Flag-ALKBH2 and treated with MMS ± 2 μM CDDP. **(F)**
1053 Alkaline comet assay of H1299 cells treated with MMS (50 μM) and/or CDDP (2 μM); tail
1054 moments were quantified from 70 cells. The experiment was repeated twice with similar results.
1055 **(G, H)** IC_{50} analysis of CDDP in H1299 (F) and H460 (G) cells with MMS co-treatment. **(I)**
1056 Representative images of clonogenic survival of H460 cells treated with MMS (75 μM) and CDDP
1057 (2 μM), and **(J)** colony quantification. Colony numbers were averaged from 3 plates per
1058 experiment (N = 3), and the assay was repeated twice with similar results. **(K, L)** 3D tumor
1059 spheroid growth of H1299 cells treated with MMS (100 μM) and CDDP (2 μM); Calcein-AM (live

1060 cells)/PI (dead cells) staining (K) and spheroid volume quantification (L). Data points represent
1061 individual spheroids from one representative experiment (n = 4 per condition); spheroid assays
1062 were independently repeated twice with similar results. Scale bar = 200 μm. For CCK-8 and IC_{50}
1063 assays (A, D, E, G, H), data points represent technical replicates from one representative
1064 experiment (three wells per condition, four wells in panel E); each experiment was independently
1065 repeated twice with similar results. Error bars indicate mean ± SD. Statistical comparisons were
1066 performed using unpaired two-tailed Student's *t*-tests; comet assay data in (E) were analyzed using
1067 the Mann–Whitney test. NS, not significant.
1068
1069 **Figure 8. Model of the biphasic TRIM28–ALKBH2 regulatory switch induced by alkylation**
1070 **stress. (I) Basal state.** MAGEA6-assisted, TRIM28-dependent K48-linked ubiquitination limits
1071 ALKBH2, while ALKBH2 increases TRIM28 transcription and protein levels. **(II) Acute**
1072 **alkylation stress:** MMS enhances TRIM28–ALKBH2 association, further facilitated by
1073 MAGEA6, leading to accelerated ALKBH2 ubiquitination and degradation. **(III) Prolonged**
1074 **alkylation stress:** Ubiquitination progressively targets TRIM28, promoting its degradation and
1075 relieving ubiquitin-dependent suppression of ALKBH2. Together with MMS-induced
1076 transcriptional upregulation of ALKBH2, this shift results in a time-dependent accumulation of
1077 ALKBH2 protein.

Figure 1 (Sun et al.)

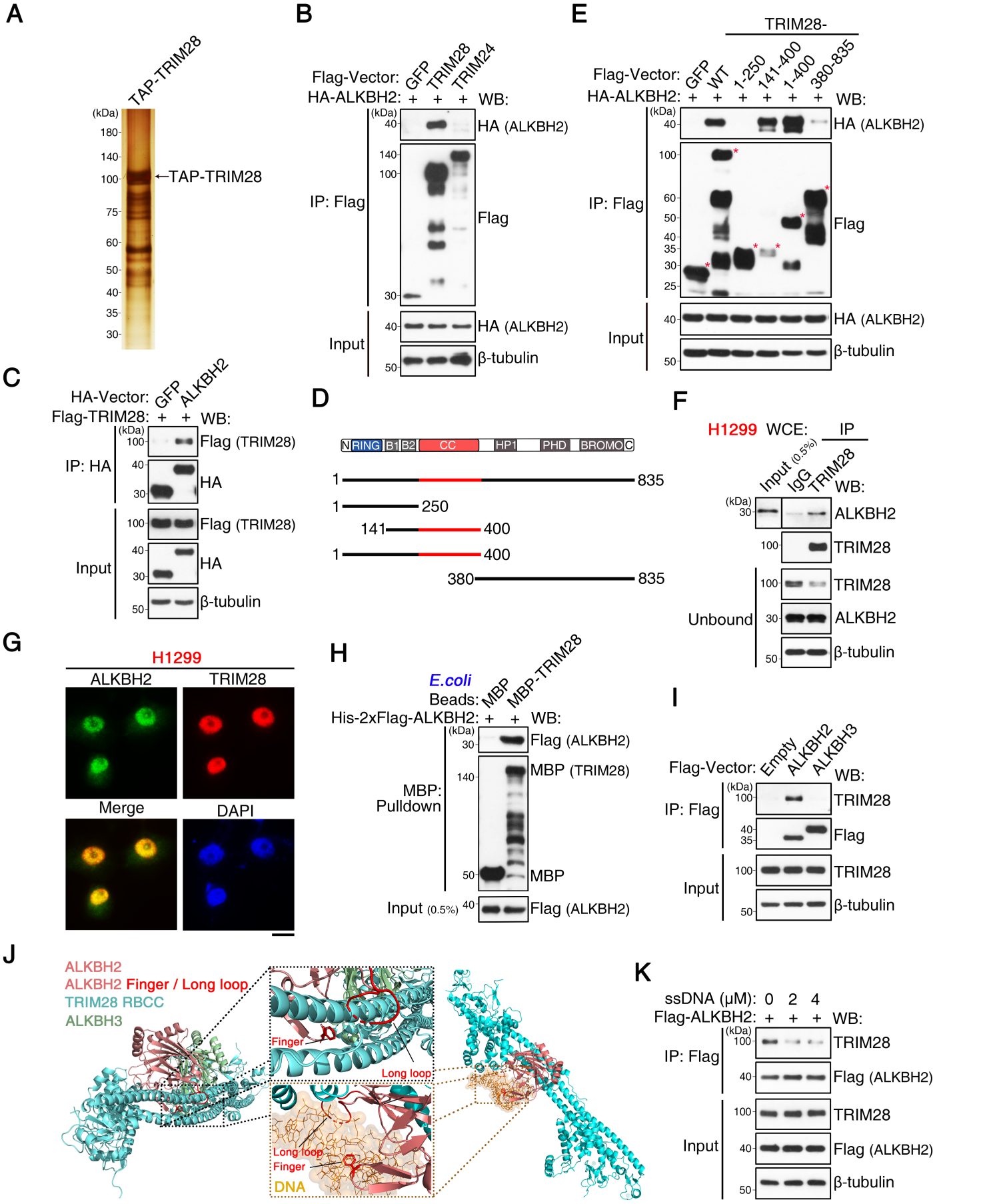

Figure 2 (Sun et al.)

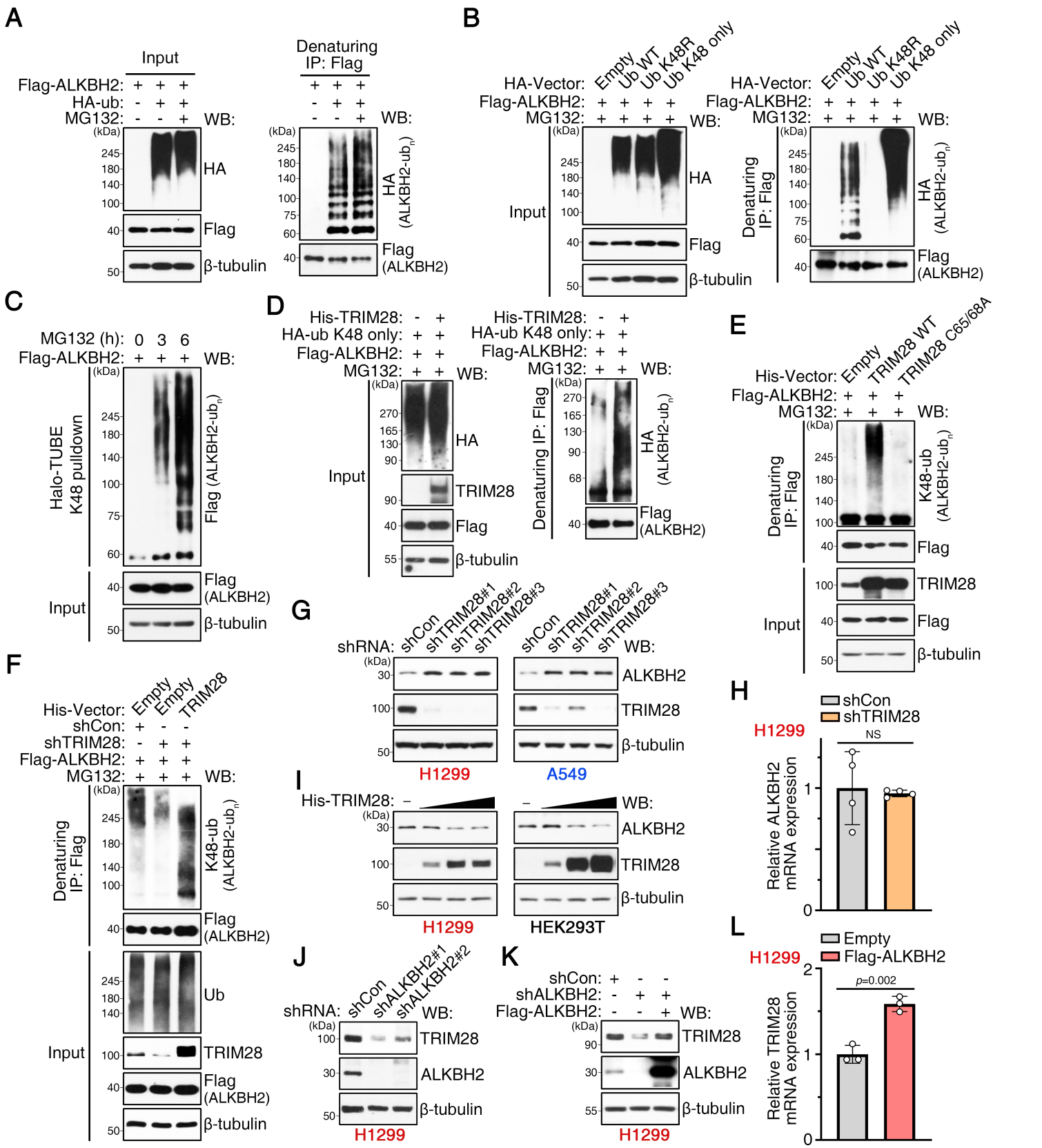

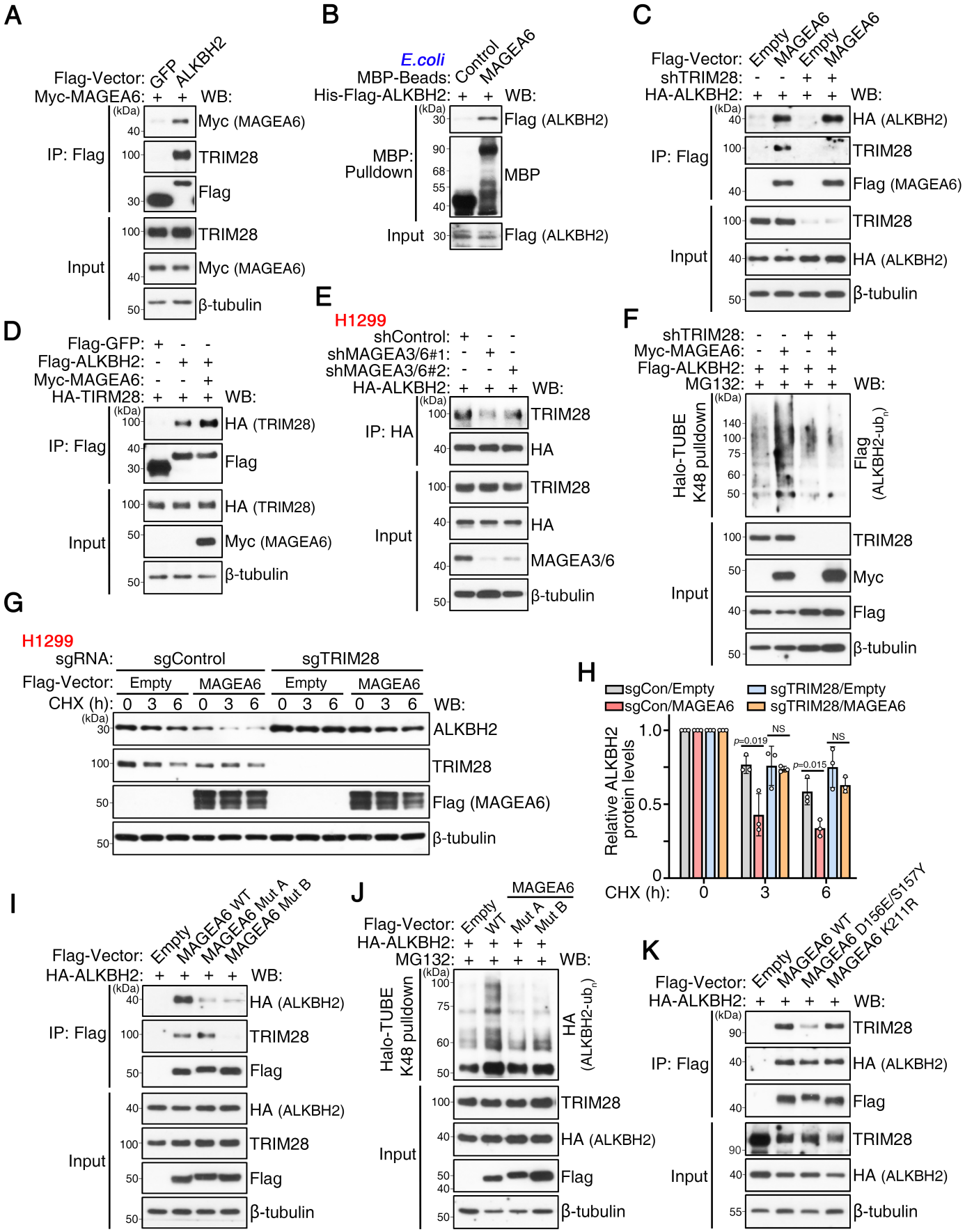
A
Flag-Vector: GFP ALKBH2
Myc-MAGEA6: + + WB:
IP: Flag
Input
Myc (MAGEA6)
TRIM28
Flag
β-tubulin
B
E.coli
MBP-Beads: Control MAGEA6
His-Flag-ALKBH2: + + WB:
MBP: Pulldown
Input
Flag (ALKBH2)
MBP
C
Flag-Vector: Empty MAGEA6 Empty MAGEA6
shTRIM28: - - + +
HA-ALKBH2: + + + + WB:
HA (ALKBH2)
Flag (MAGEA6)
D
Flag-GFP: + - -
Flag-ALKBH2: - + +
Myc-MAGEA6: - - +
HA-TIRM28: + + + WB:
HA (TRIM28)
Myc (MAGEA6)
E
H1299
shControl: + - -
shMAGEA3/6#1: - + -
shMAGEA3/6#2: - - +
HA-ALKBH2: + + + WB:
IP: HA
HA
MAGEA3/6
F
shTRIM28: - - + +
Myc-MAGEA6: - + - +
Flag-ALKBH2: + + + +
MG132: + + + + WB:
Halo-TUBE K48 pulldown
Flag (ALKBH2-ub$_n$)
Myc
G
H1299
sgRNA: sgControl sgTRIM28
Flag-Vector: Empty MAGEA6 Empty MAGEA6
CHX (h): 0 3 6 0 3 6 0 3 6 0 3 6 WB:
ALKBH2
Flag (MAGEA6)
H
sgCon/Empty
sgCon/MAGEA6
sgTRIM28/Empty
sgTRIM28/MAGEA6
Relative ALKBH2 protein levels
p=0.019
p=0.015
NS
CHX (h): 0 3 6
I
Flag-Vector: Empty MAGEA6 WT MAGEA6 Mut A MAGEA6 Mut B
HA-ALKBH2: + + + + WB:
J
MAGEA6
Flag-Vector: Empty WT Mut A Mut B
HA-ALKBH2: + + + +
MG132: + + + + WB:
K
Flag-Vector: Empty MAGEA6 WT MAGEA6 D156E/S157Y MAGEA6 K211R
HA-ALKBH2: + + + + WB:

Figure 4 (Sun et al.)

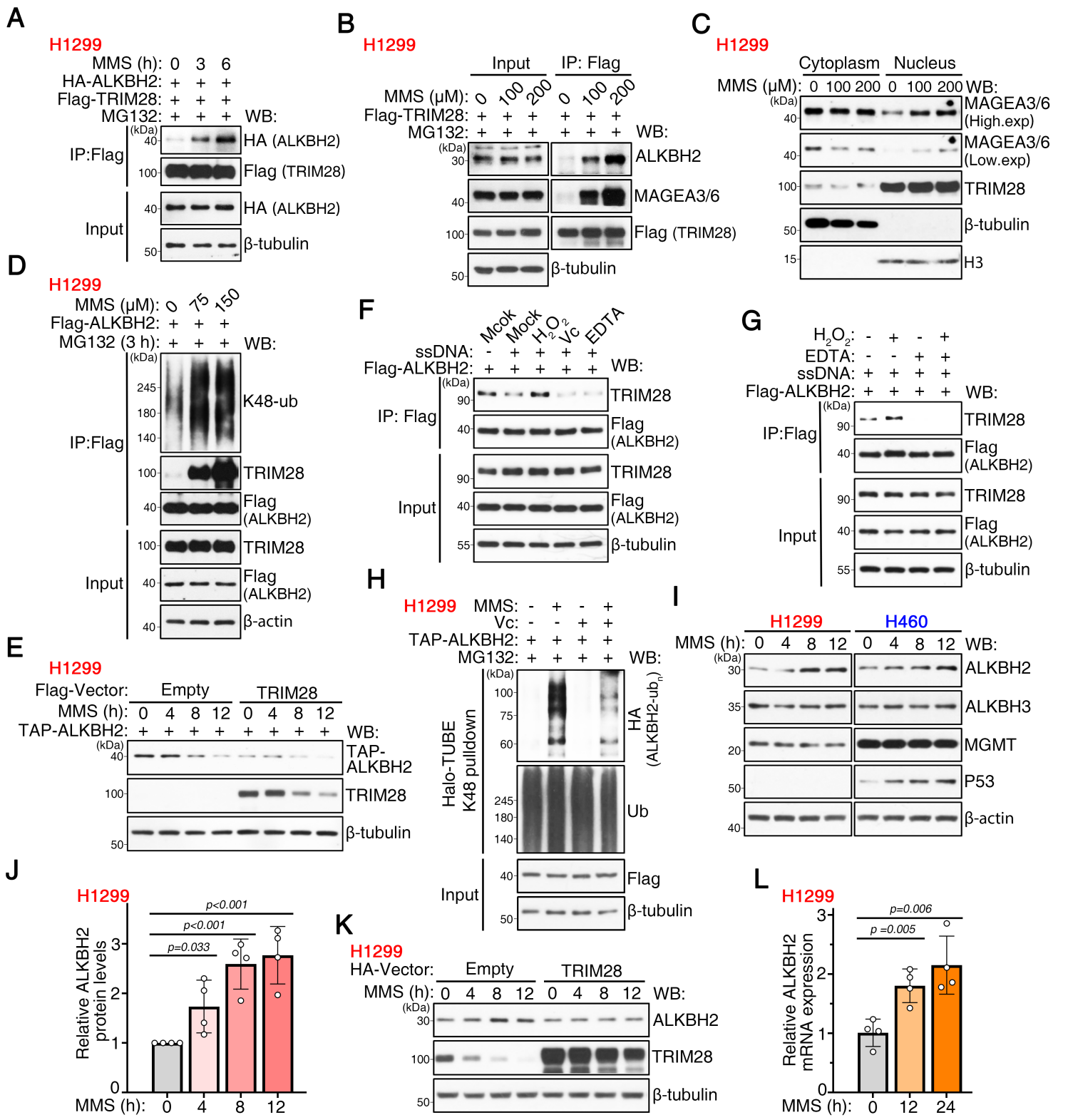

Figure 5 (Sun et al.)

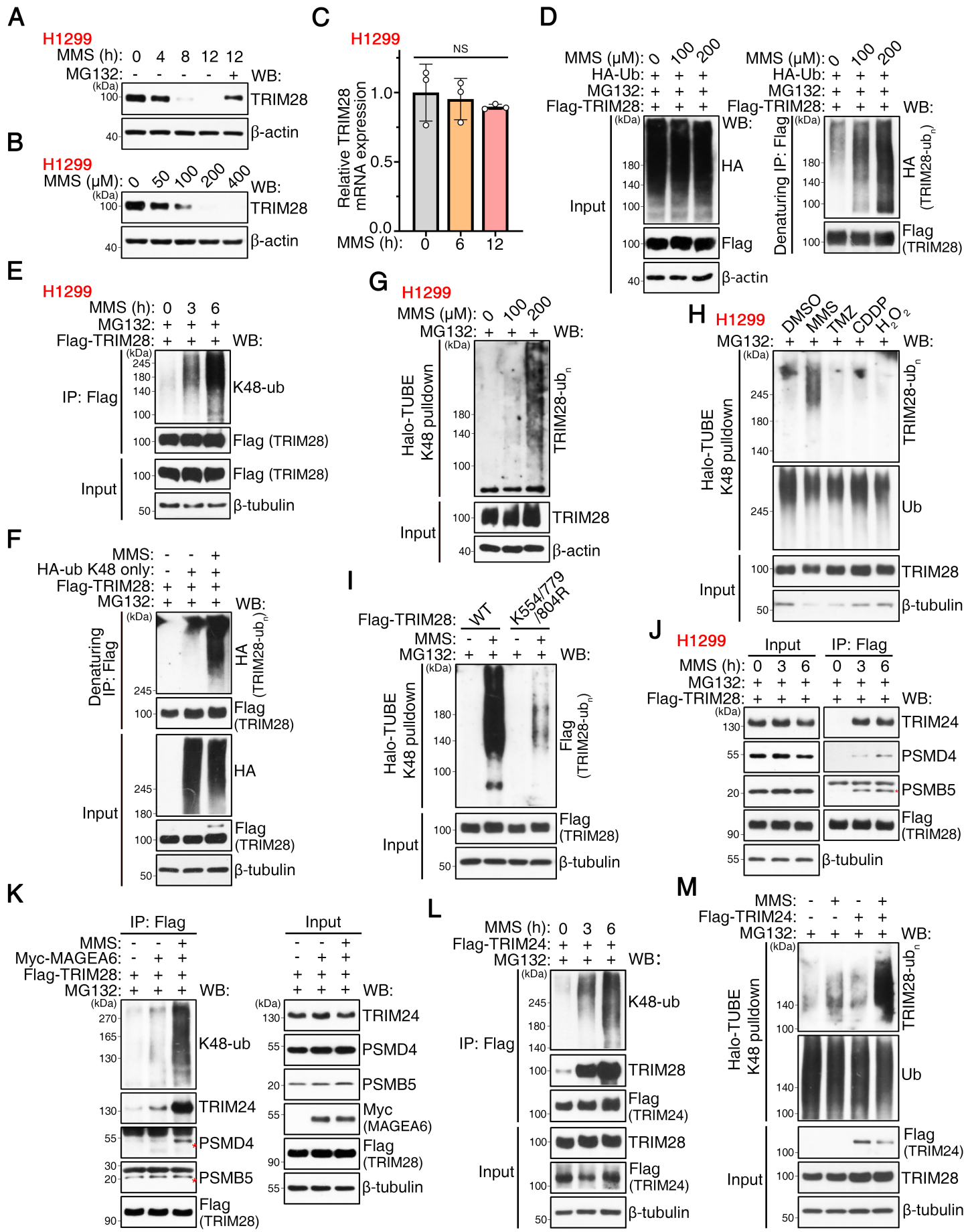

Figure 6 (Sun et al.)

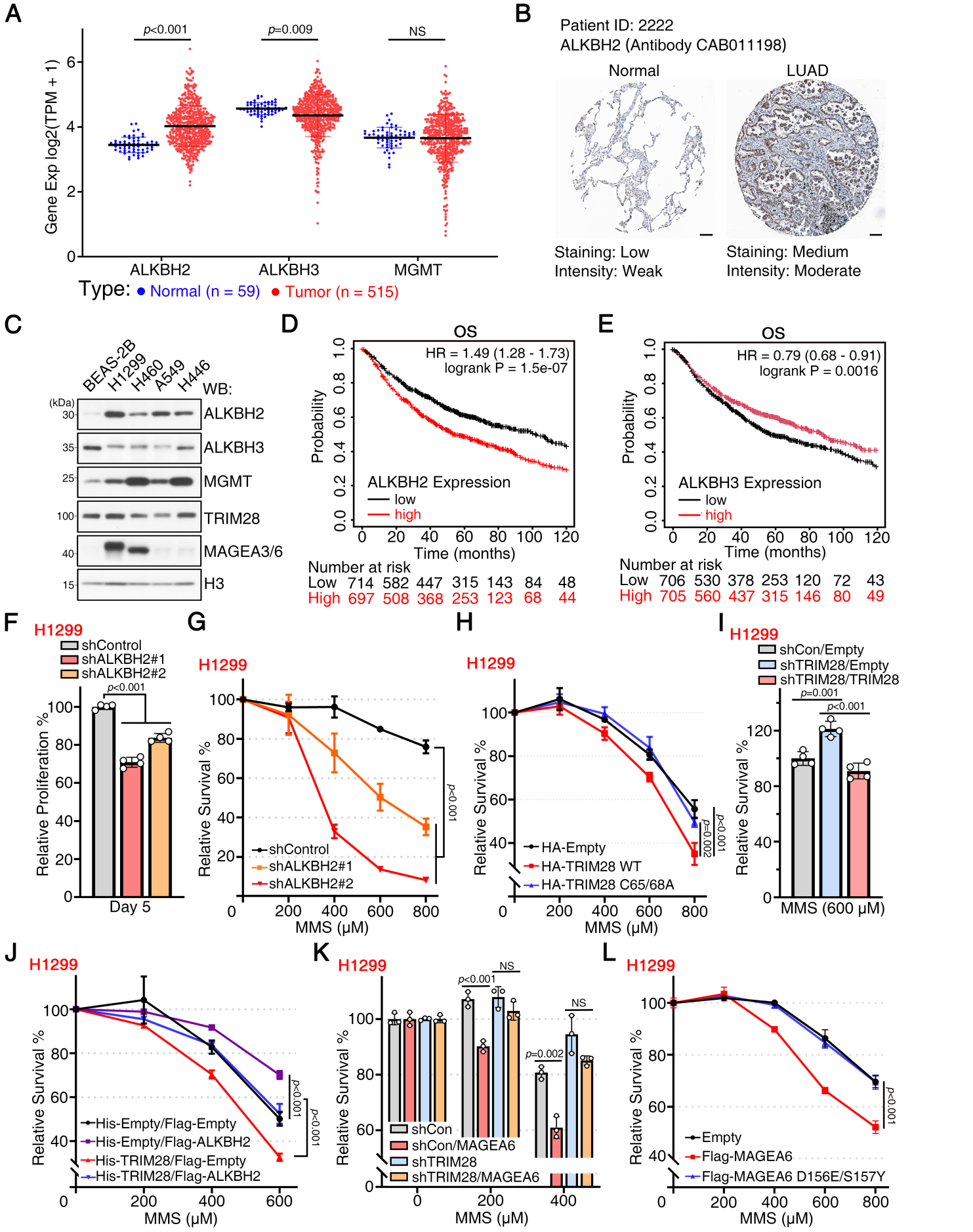

Figure 7 (Sun et al.)

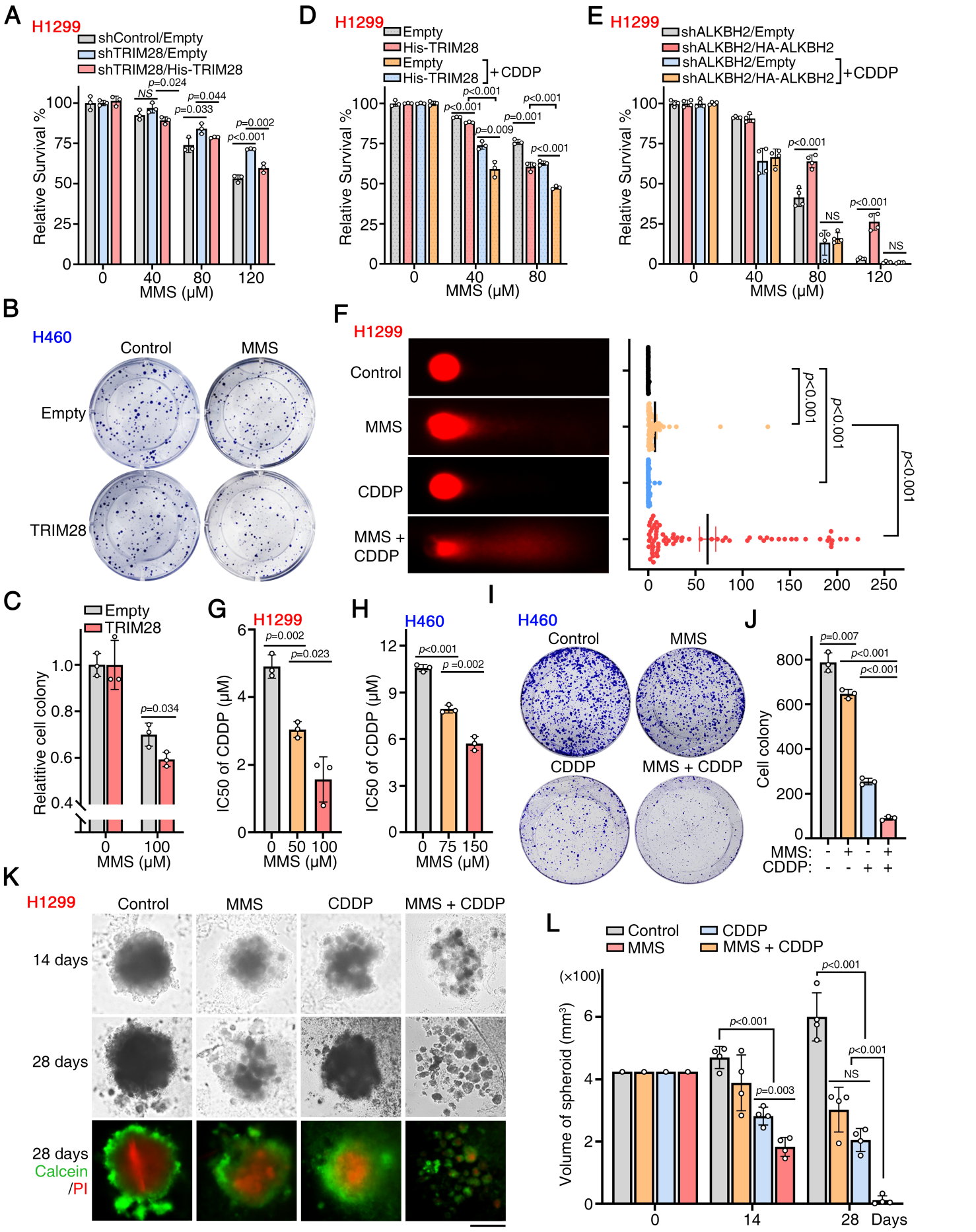
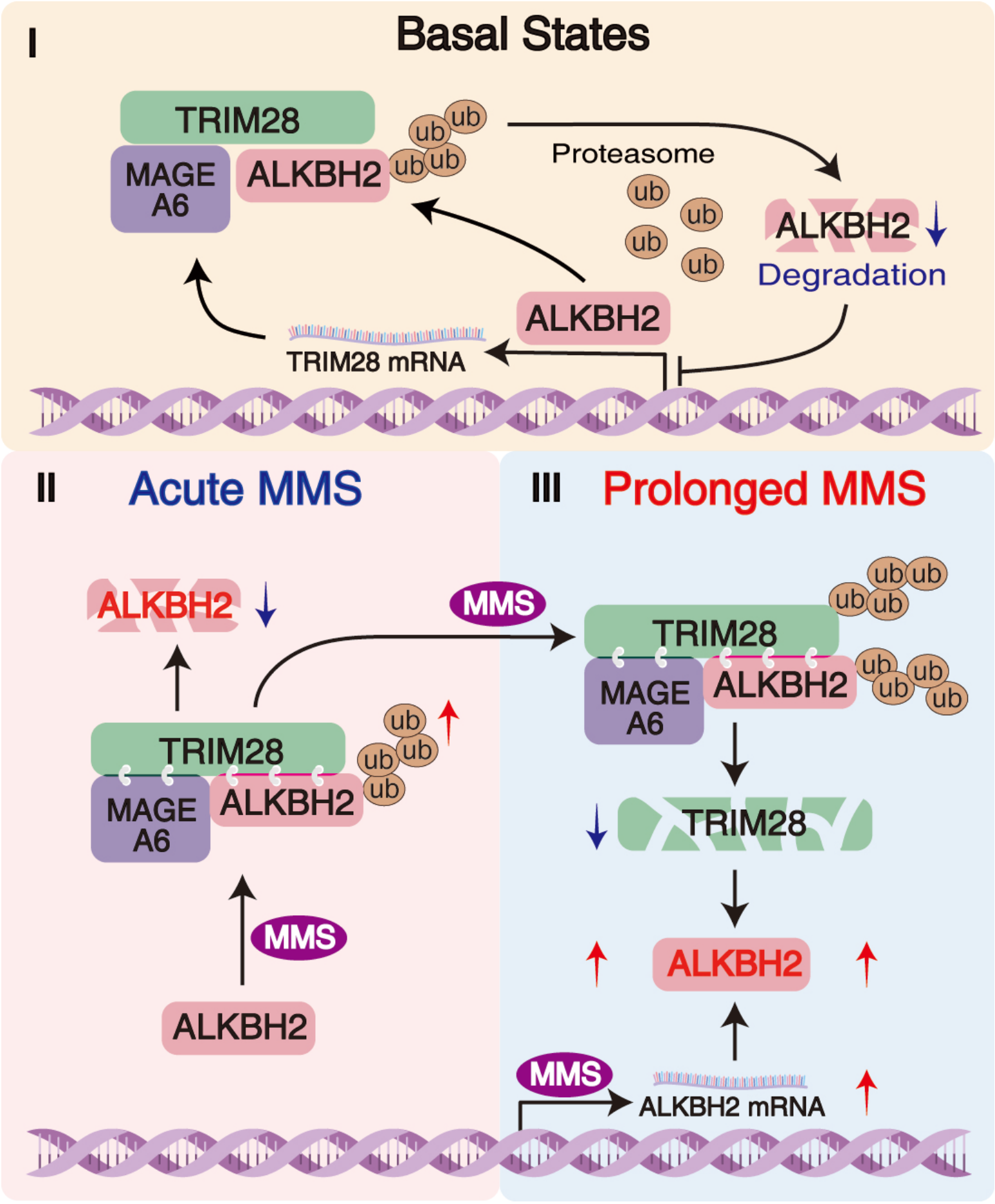
Figure 8 (Sun et al.)